Supporting Information

Structure, absolute configuration, and conformational study of resorcylic acid derivatives and related congeners from the fungus *Penicillium brocae*†

Peng Zhang,‡[ab] Ling-Hong Meng,‡[ab] Attila Mándi,[c] Xiao-Ming Li,[a] Tibor Kurtán*[c] and Bin-Gui Wang*[a]

Content

SI-1: Conformational analysis and TDDFT-ECD calculations of compounds **1** and **3**.

The ECD spectrum of **1** in acetonitrile showed negative Cotton effects (CEs) at 307 and 212 nm and positive ones at 285, 260 and 227 nm. The initial MMFF conformational analysis of the arbitrarily chosen (14*S*)-**1** afforded 74 MMFF conformers, which were reoptimized at B3LYP/6-31G(d) level of theory *in vacuo* resulting in eight conformers over 2% Boltzmann population (Figure 1) and at B97D/TZVP level[1,2] with PCM solvent model for acetonitrile resulting in 10 low-energy conformers (Figure 2).

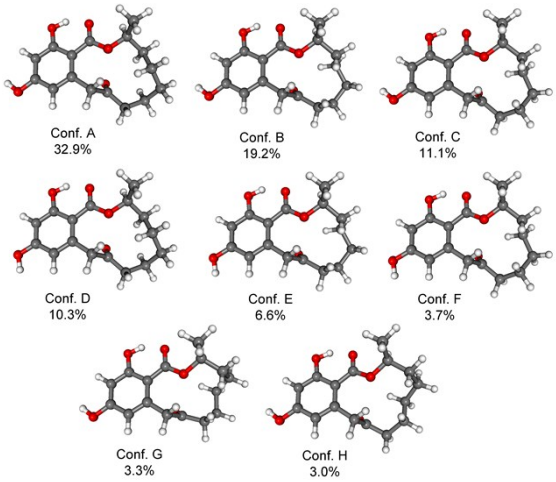

Figure 1. Structures and populations of the low-energy B3LYP/6-31G(d) *in vacuo* conformers (> 2%) of (14*S*)-**1**.

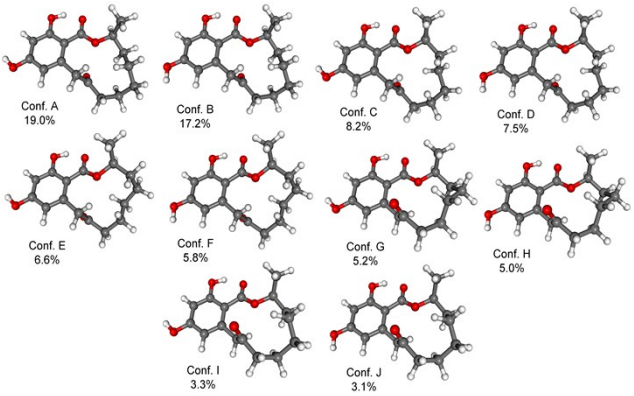

Figure 2. Structures and populations of the low-energy B97D/TZVP PCM/MeCN conformers (> 2%) of (14*S*)-**1**.

In conformers A−F of the B97D/TZVP reoptimization, the C-8 carbonyl group has similar orientation relative to the resorcylic acid chromophore and the 14-Me group adopted *quasi-axial* orientation, while they differed in the orientation of the 4-OH proton and C-10−13 methylene groups. In accordance they showed very similar computed ECD spectra, which were mirror image of the experimental curve. The C-8 carbonyl was flipped in conformers G−J, which as a consequence gave different computed ECD spectra from those of conformers A−F. Conformers G−J were not obtained in the gas phase B3LYP/6-31G(d) conformational analysis (Figure 1). The Boltzmann-averaged ECD spectra calculated for both the *in vacuo* and solvent model conformers at B3LYP/TZVP, BH&HLYP/TZP and PBE0/TZVP levels were mirror image of the experimental ECD spectrum allowing the determination of the absolute configuration as (14*R*) (Figures 3 and 4). The solvent model and more advanced functional were able to improve the agreement significantly. The best agreement was found for the BH&HLYP computed averaged ECD spectrum of the solvent model conformers, which is shown in Figure 3.

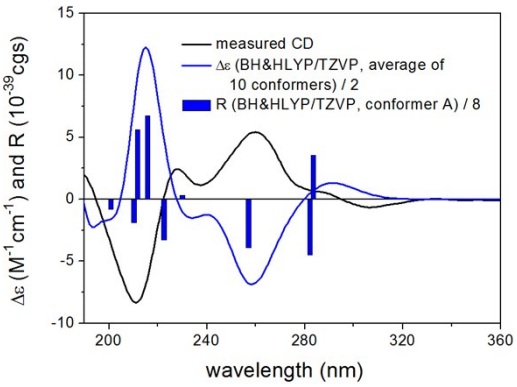

Figure 3. Experimental ECD spectrum of **1** in acetonitrile compared with the Boltzmann-weighted BH&HLYP/TZVP ECD spectrum calculated for the B97D/TZVP (PCM model for MeCN) conformers of (14*S*)-**1**. Bars represent rotational strength values for the lowest-energy conformer.

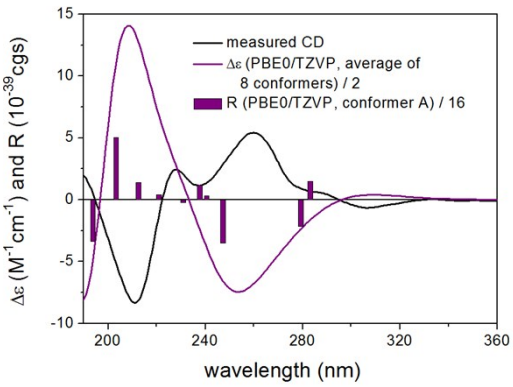

Figure 4. Experimental ECD spectrum of **1** in acetonitrile compared with the Boltzmann-weighted PBE0/TZVP ECD spectrum calculated for the B3LYP/6-31G(d) *in vacuo* conformers of (14*S*)-**1**. Bars represent rotational strength values for the lowest-energy conformer.

Compared to (*R*)-dihydroresocylide (**1**), compound **3** had an additional stereogenic centre at C-10 due to the *sec*-hydroxyl group. The corresponding CEs in the ECD spectra of **1** and **3** had the same sign except for the 285 nm positive shoulder of **1**, which was changed to a negative shoulder in **3**. Similarly to the case of **1**, *in vacuo* B3LYP/6-31G(d) and B97D/TZVP PCM solvent model (MeCN) reoptimization of the initial MMFF conformers of (10*R*,14*R*)-**3** were carried out to reveal the effect of the additional C-10 stereogenic centre on the preferred conformation. B97D/TZVP PCM solvent model (MeCN) reoptimization of (10*R*,14*R*)-**3** afforded 17 conformers above 2.0% population (Figure 5), in all of which the 14-Me group had *quasi-equatorial* orientation and the orientation of the C-8 carbonyl group was similar to those of the high-energy conformers G−J of **1**.

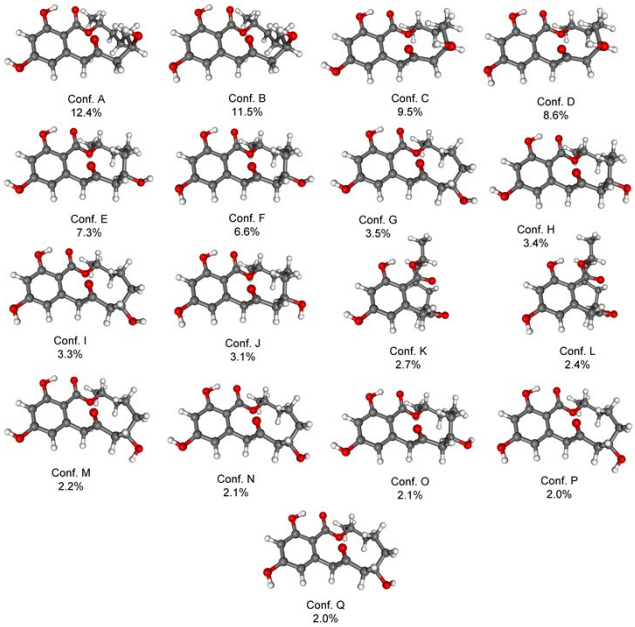

Figure 5. Structure and population of the low-energy B97D/TZVP PCM/MeCN conformers (> 2%) of (10*R*,14*R*)-**3**.

In the low-energy conformers A−D totaling 42.0% population, the 10-OH was axial and hydrogen-bonded to the C-8 carbonyl oxygen, while the C-10 was flipped in the higher-energy conformers E−Q (42.7% total population) shifting the 10-OH to a *quasi-equatorial* position. Interestingly, this conformational change of the macrolactone ring did not result in significant changes in the computed ECD spectra of the conformers. The Boltzmann-weighted ECD spectra of the B97D/TZVP (PCM solvent model for MeCN) conformers of (10*R*,14*R*)-**3** reproduced well the experimental ECD curve of **3** with BH&HLYP PCM/MeCN affording the best agreement (Figure 6), which confirmed the (10*R*,14*R*) absolute configuration of **3**.

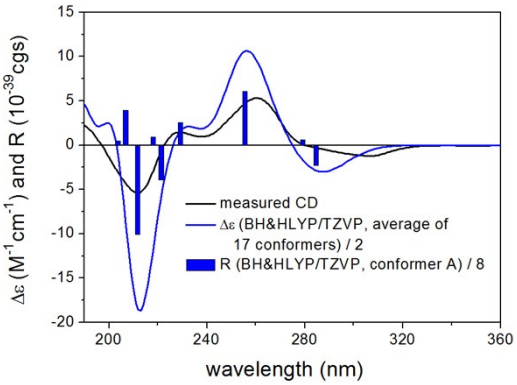

Figure 6. Experimental ECD spectrum of **3** in acetonitrile compared with the Boltzmann-weighted BH&HLYP/TZVP spectrum calculated for the B97D/TZVP (PCM model for MeCN) conformers of (10*R*,14*R*)-**3**. Bars represent rotational strength values for the lowest-energy conformer.

SI-2: Solid-state TDDFT-ECD calculation of **3**.

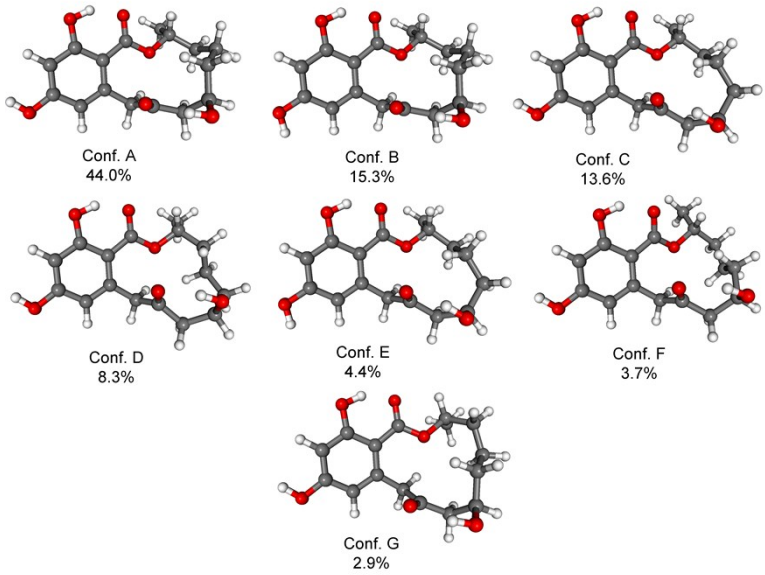

Figure 7. Structure and population of the low-energy B3LYP/6-31G(d) *in vacuo* conformers (> 2%) of (10*R*,14*R*)-**3**.

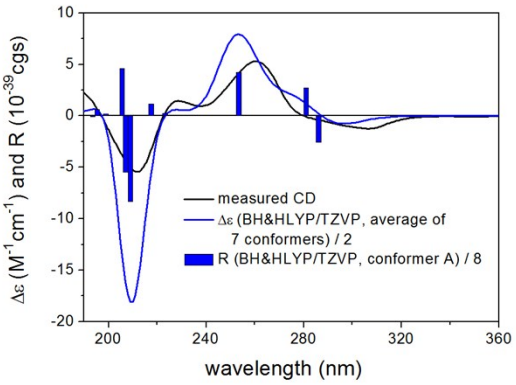

Figure 8. Experimental ECD spectrum of **3** in acetonitrile compared with the Boltzmann-weighted BH&HLYP/TZVP spectrum calculated for the B3LYP/6-31G(d) *in vacuo* conformers of (10*R*,14*R*)-**3**. Bars represent rotational strength values for the lowest-energy conformer.

The *in vacuo* B3LYP/6-31G(d) conformers (Figure 7) of **3** provided also satisfactory agreement (Figure 8), which were not improved significantly by the more advanced functional, larger basis set and solvent model. The calculations showed that although the additional C-10

stereogenic centre induces remarkable conformational changes of the macrolactone ring, these changes are not reflected profoundly in the ECD spectra of the conformers. The single crystal X-ray of **3**[3] could be also resolved, which showed the presence of two conformers in 1:1 ratio in the crystal lattice (Figure 9).

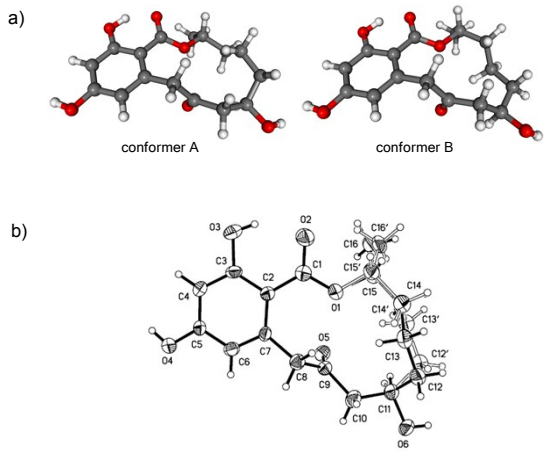

Figure 9. a) Structures of the solid-state X-ray conformers observed in 1:1 ratio in the crystal lattice. b) X-ray structure of **3** (Note: A different numbering system is used for the structure in the text).

Given the geometry of the solid-state conformers, the solid-state TDDFT-ECD approach[4,5] could be applied. This method has been used efficiently to determine the absolute configuration of natural products, for which the X-ray analysis reported only the relative configuration.[2,4−6] Moreover, it was also found useful to compare the solution and solid-state conformers of conformationally flexible molecules.[7,8] In the two solid-state conformers of **3** differing in the flip of the C-12 methylene, the 14-Me and 10-OH were *quasi-equatorial*, similar to the computed conformers E−H, but the C-8 carbonyls had different orientation. The two solid-state conformers were not represented by any of the computed solution conformers A−Q above 2% population and their macrolactone rings were more flattened and extended than those in most of the computed conformers. The solid-state ECD spectrum of **3** recorded as KCl disc showed the same signs for the CEs of the corresponding ECD bands as those of the solution ECD but the two high-wavelength negative CEs had much larger amplitude relatively to that of the positive band. ECD spectra were calculated for the two solid-state conformers with different methods and the weighted average ECD spectra reproduced well the signs of the CEs confirming the (10*R*,14*R*) absolute configuration but the relative intensity of the 230 nm positive shoulder was overestimated (Figure 10).

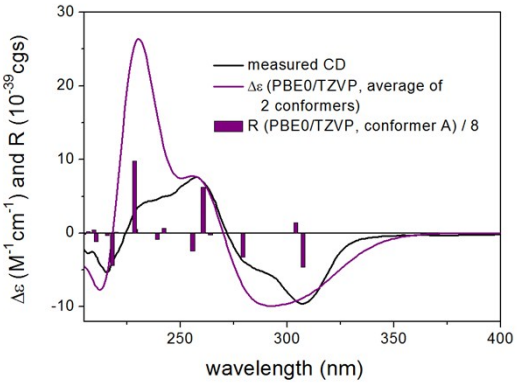

Figure 10. Experimental solid-state ECD spectrum of **3** as KCl disc compared with the PBE0/TZVP spectrum calculated for the two solid-state X-ray conformers of (10*R*,14*R*)-**3**. Bars represent rotational strength values for conformer A.

X-ray crystallographic analysis of compound 3

Colorless prismatic crystals of **3** were obtained by recrystallization from MeOH. $C_{17}H_{24}O_7$, M_r = 340.36, monoclinic space group *P*2(1), unit cell dimensions a = 8.0269(8) Å, b = 12.6458(10) Å, c = 16.8180(18) Å, V = 1707.1(3) Å^3, α = β = γ = 90°, Z = 4, d_{calcd} = 1.324 mg/m^3, crystal dimensions 0.26 × 0.18 × 0.12 mm, μ = 0.860 mm^{-1}, F(000) = 728. The 3524 measurements yielded 2485 independent reflections after equivalent data were averaged, and Lorentz and polarization corrections were applied. The final refinement gave R_1 = 0.0810 and wR_2 = 0.2009 [I >2σ(I)]. The absolute structure parameter was 0.0(7). All crystallographic data were collected on a Bruker Smart-1000 CCD diffractometer equipped with graphite-monochromated Cu Kα radiation (λ = 1.54178 Å) at 293(2) K. The data were corrected for absorption by using the program SADABS. The structure was solved by direct methods with the SHELXTL software package. All non-hydrogen atoms were refined anisotropically. The H atoms were located by geometrical calculations, and their positions and thermal parameters were fixed during the structure refinement. The structure was refined by full-matrix least-squares techniques.

SI-3: References.

[1] S. Grimme, *J. Comput. Chem.* 2006, **27**, 1787.
[2] P. Sun, D. X. Xu, A. Mándi, T. Kurtán, T. J. Li, B. Schulz and W. Zhang, *J. Org. Chem.* 2013, **78**, 7030.
[3] Crystallographic data of compound **3** have been deposited in the Cambridge Crystallographic Data Centre as CCDC 1047299. The data can be obtained free of charge via http://www.ccdc.cam.ac.uk/data_request/cif.
[4] G. Pescitelli, T. Kurtán and K. Krohn, *Assignment of the absolute configurations of natural products by means of solid-state electronic circular dichroism and quantum-mechanical calculations in: comprehensive chiroptical spectroscopy* (Eds.: N. Berova, P. L. Polavarapu, K. Nakanishi, R. W. Woody), John Wiley & Sons, Inc., New York, 2012, vol. 2, p. 217.
[5] G. Pescitelli, T. Kurtán, U. Flörke and K. Krohn, *Chirality*, 2009, **21** (1E), E181.
[6] T. Kurtán, R. Jia, Y. Li, G. Pescitelli and Y. W. Guo, *Eur. J. Org. Chem.,* 2012, 6722.
[7] T. Kurtán, G. Pescitelli, P. Salvadori, Á. Kenéz, S. Antus, T. Z. Illyés, L. Szilágyi and I. Szabó, *Chirality*, 2008, **20(3−4)**, 379.
[8] G. Kerti, T. Kurtán, T. Z. Illyés, K. E. Kövér, S. Sólyom, G. Pescitelli, N. Fujioka, N. Berova and S. Antus, *Eur. J. Org. Chem*. 2007, 296.

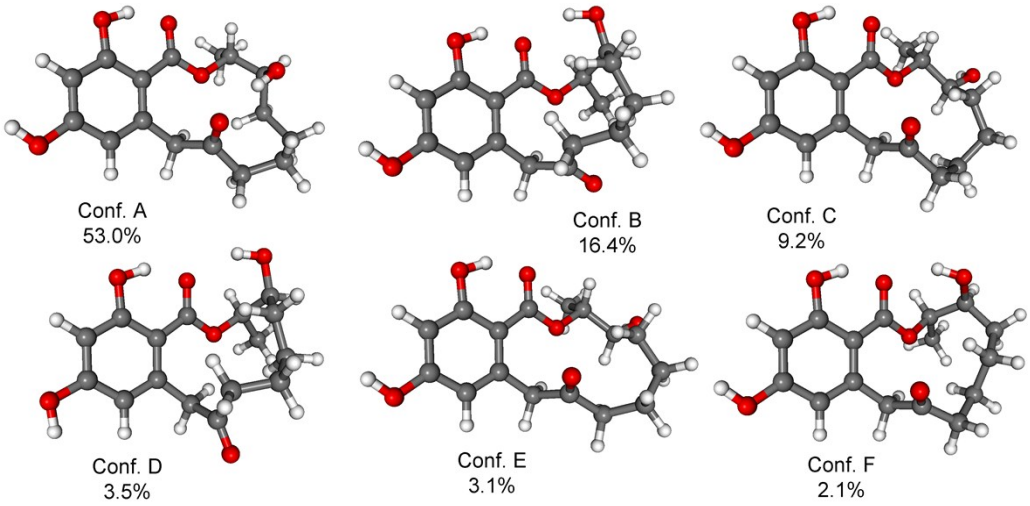

Figure S1. Structure and population of the low-energy B97D/TZVP PCM/MeCN conformers (> 2%) of (13*S*,14*R*)-**4**.

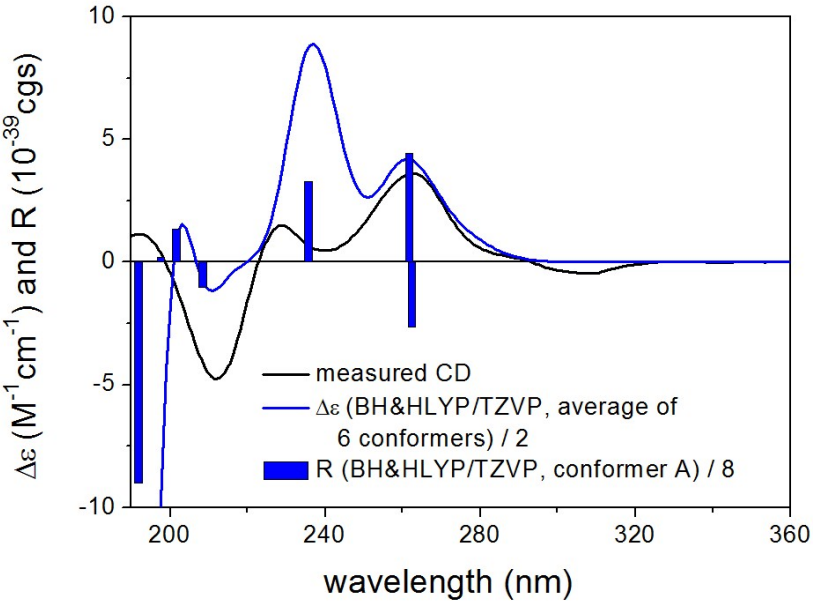

Figure S2. Experimental ECD spectrum of **4** in acetonitrile compared with the Boltzmann-weighted BH&HLYP/TZVP spectrum calculated for the B97D/TZVP (PCM for acetonitrile) conformers of (13*S*,14*R*)-**4**. Bars represent rotational strength values for the lowest-energy conformer.

Figure S3. HR-ESI-MS spectrum of compound **4**.

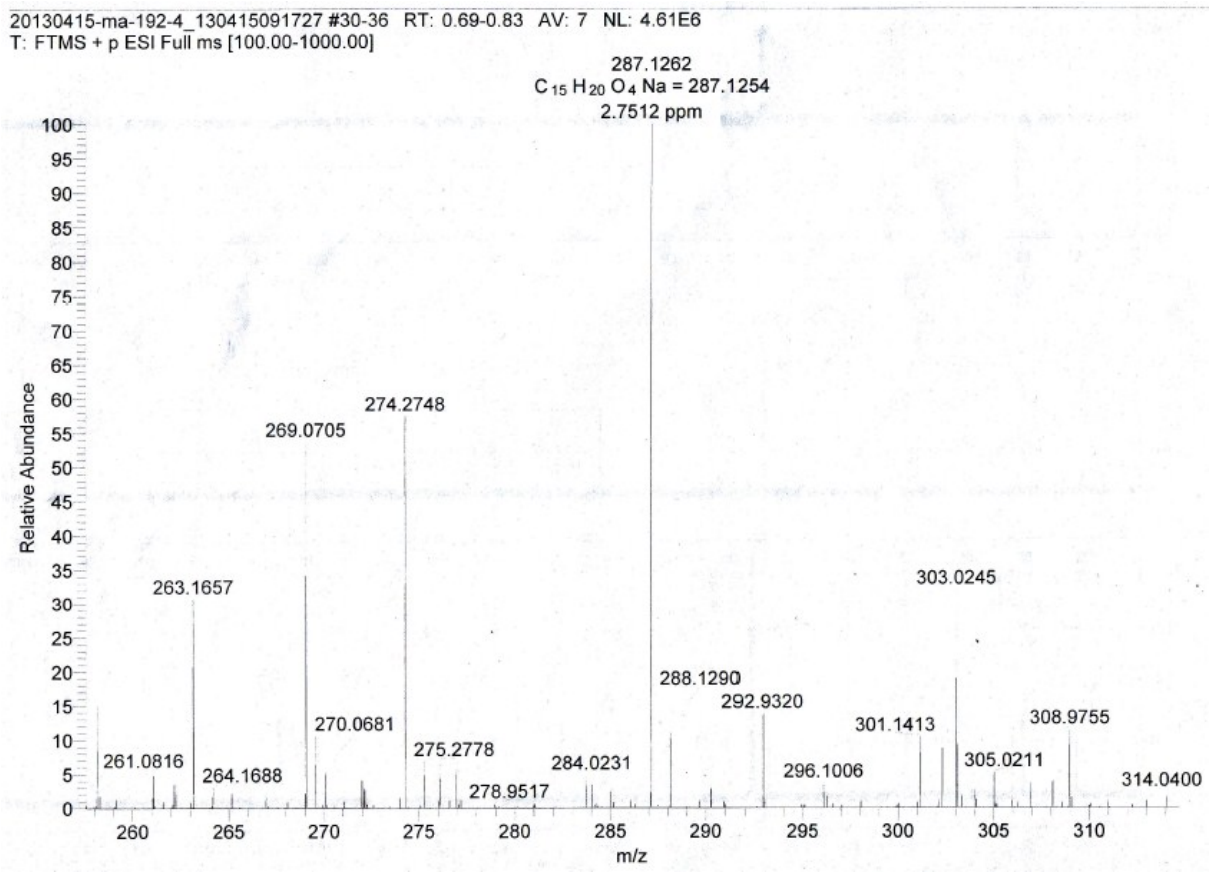

Figure S4. ^{1}H NMR (500M, DMSO-d_6) spectrum of compound **4**.

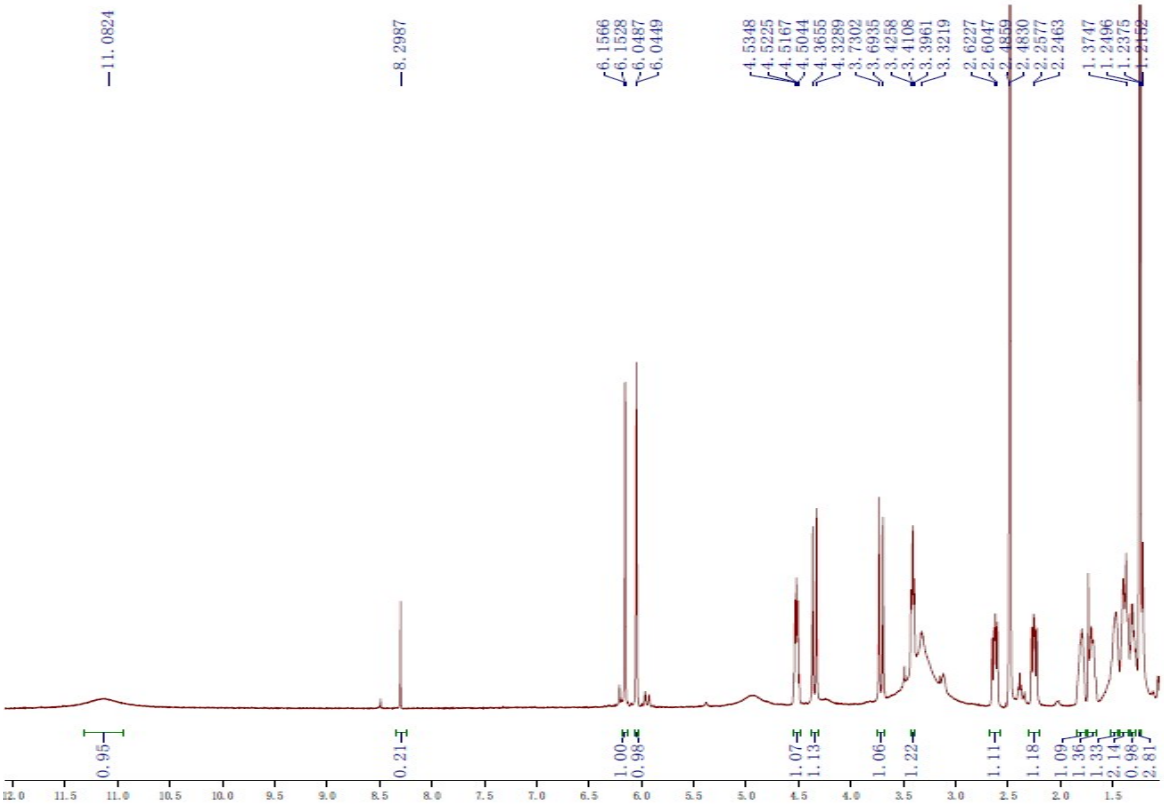

Figure S5. ^{13}C NMR (125M, DMSO-d_6) and DEPT spectra of compound **4.**

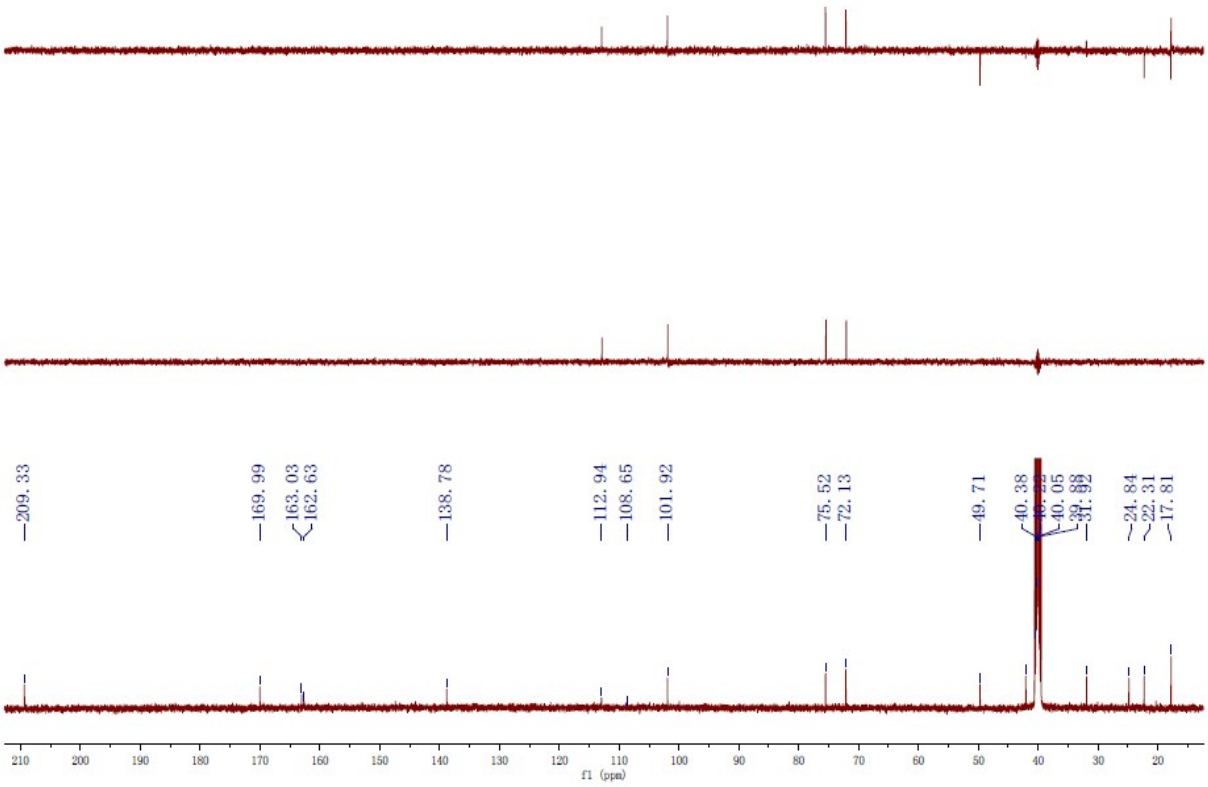

Figure S6. ^{1}H-^{1}H COSY spectrum of compound **4**.

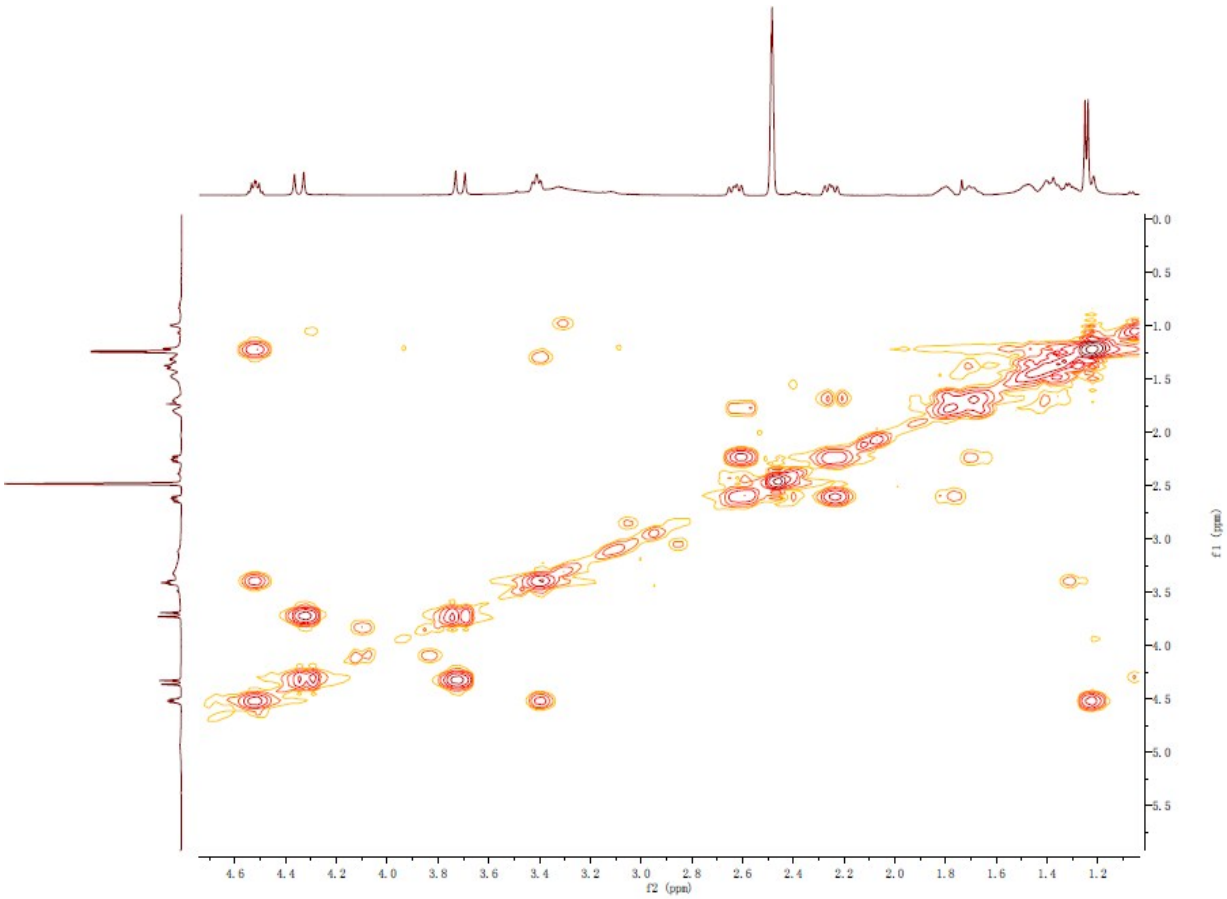

Figure S7. HSQC spectrum of compound **4**.

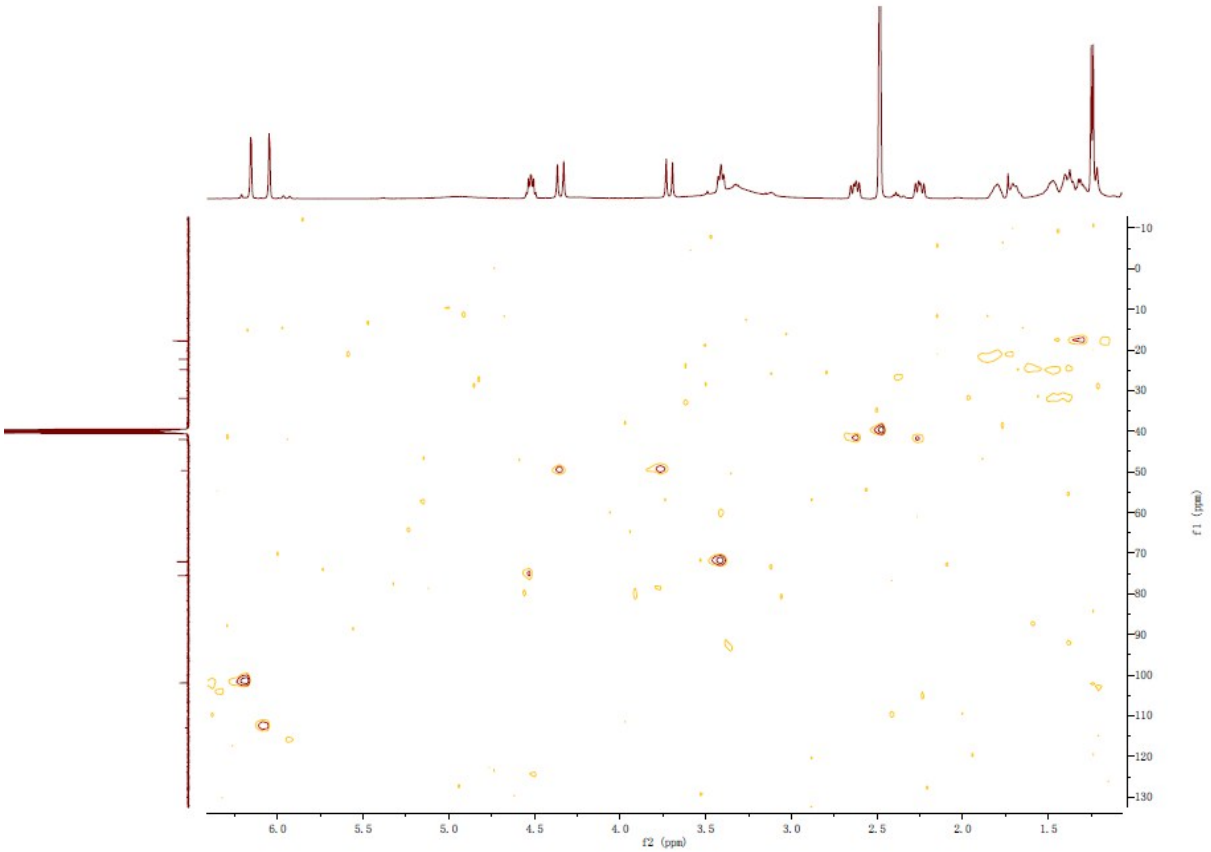

Figure S8. HMBC spectrum of compound **4**.

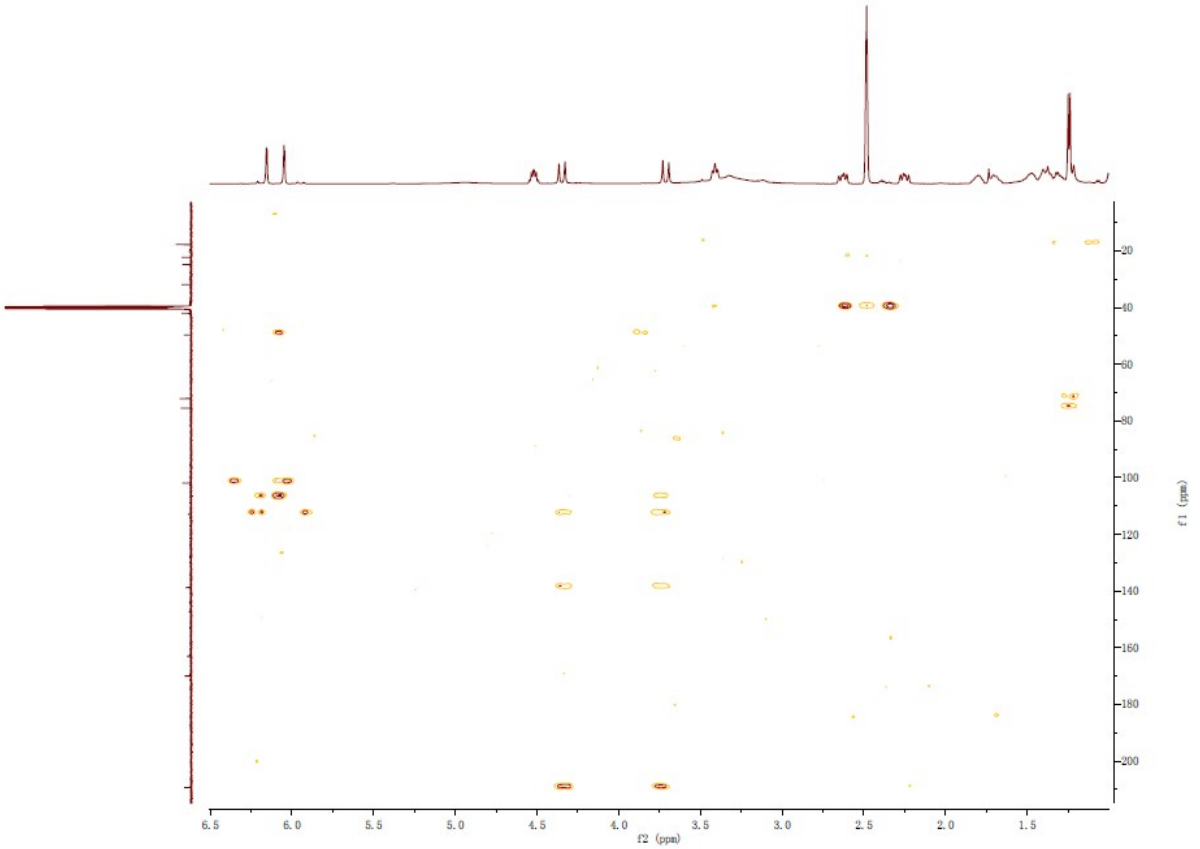

Figure S9. NOESY spectrum of compound **4**.

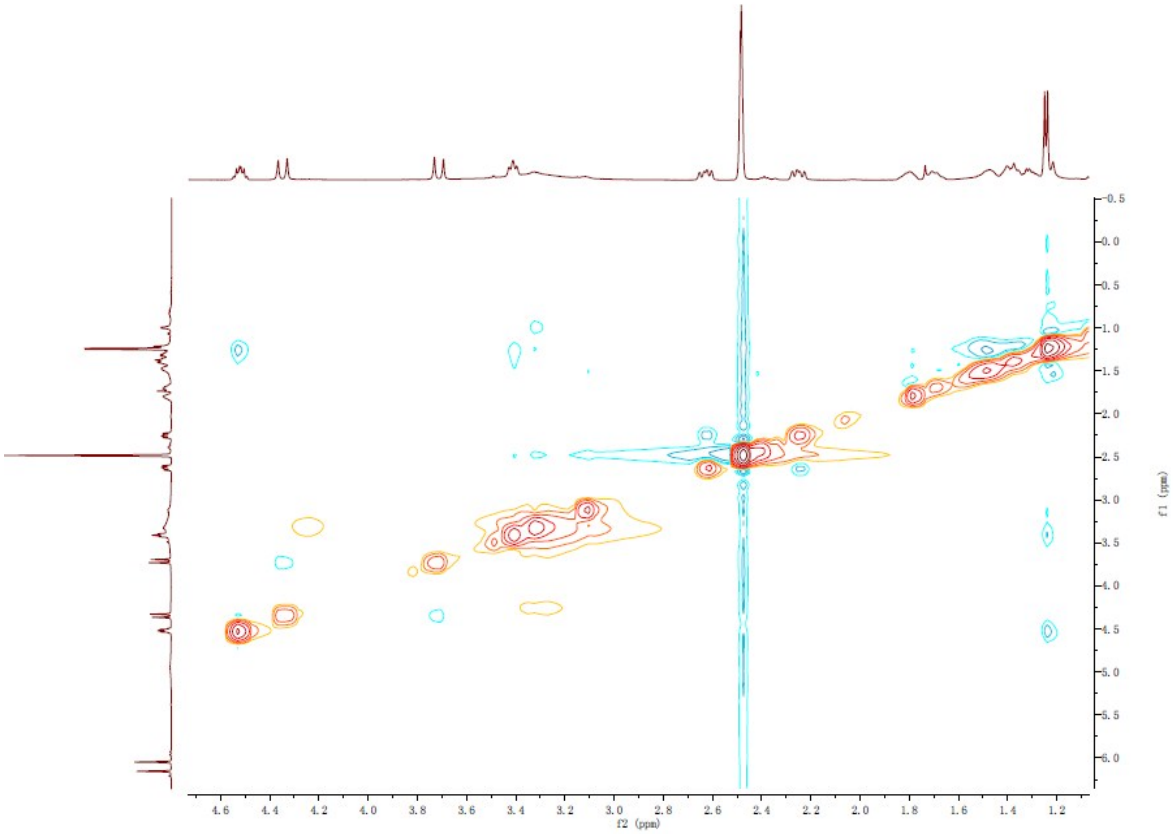

Figure S10. HR-ESI-MS spectrum of compound **5**.

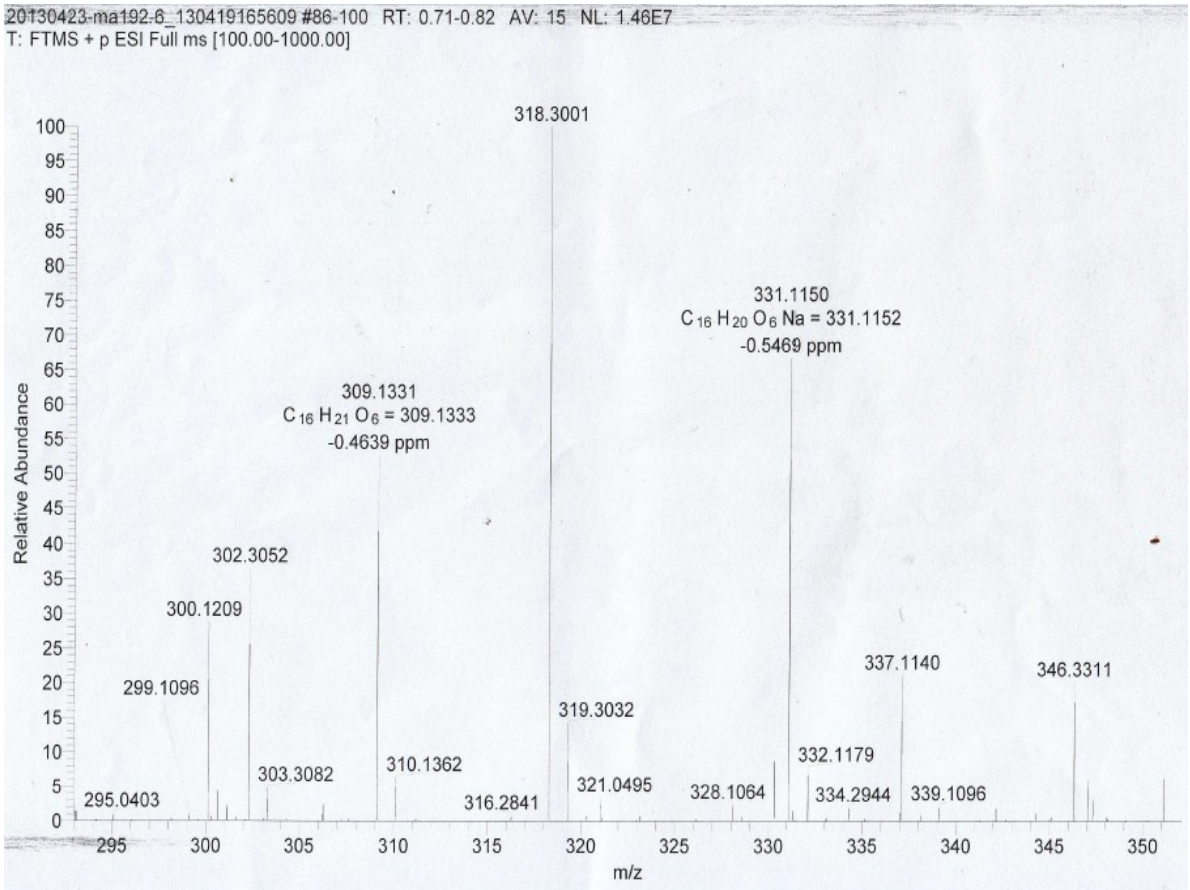

Figure S11. ^{1}H NMR (500M, $CDCl_3$) spectrum of compound **5**.

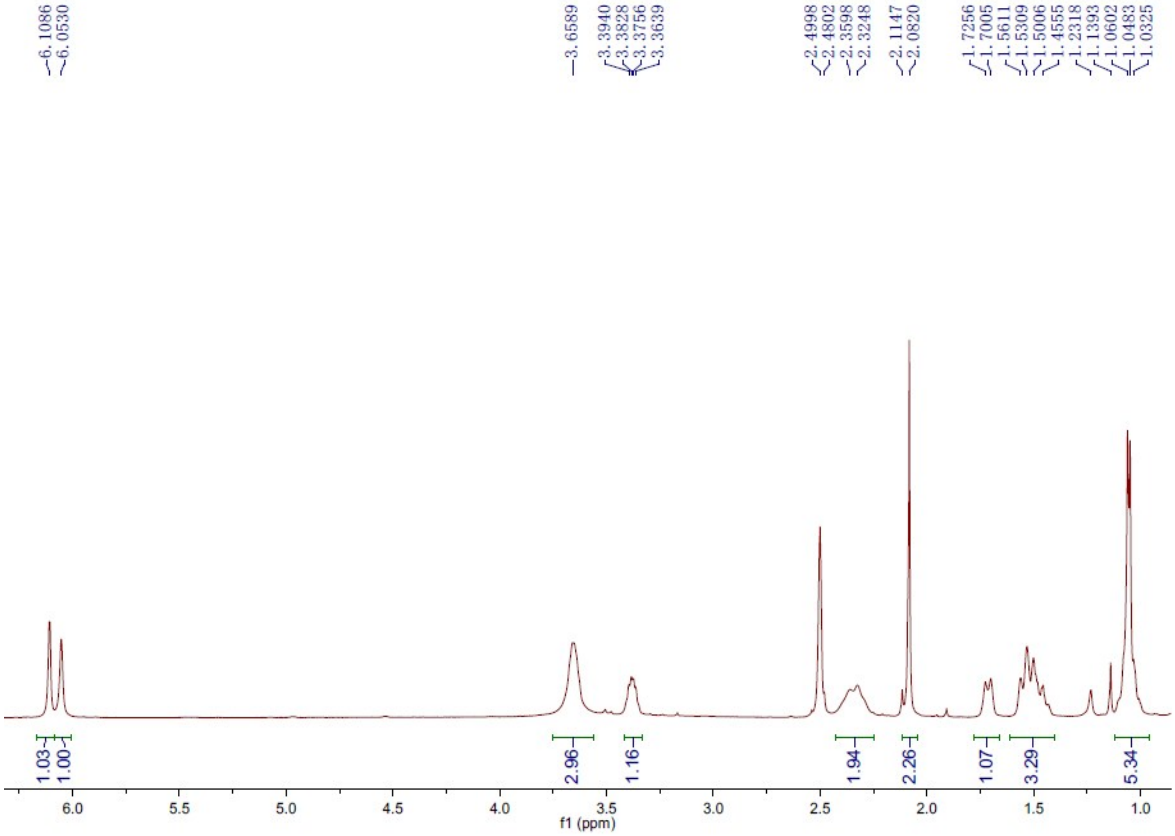

Figure S12. ^{13}C NMR (125M, $CDCl_3$) and DEPT spectra of compound **5**.

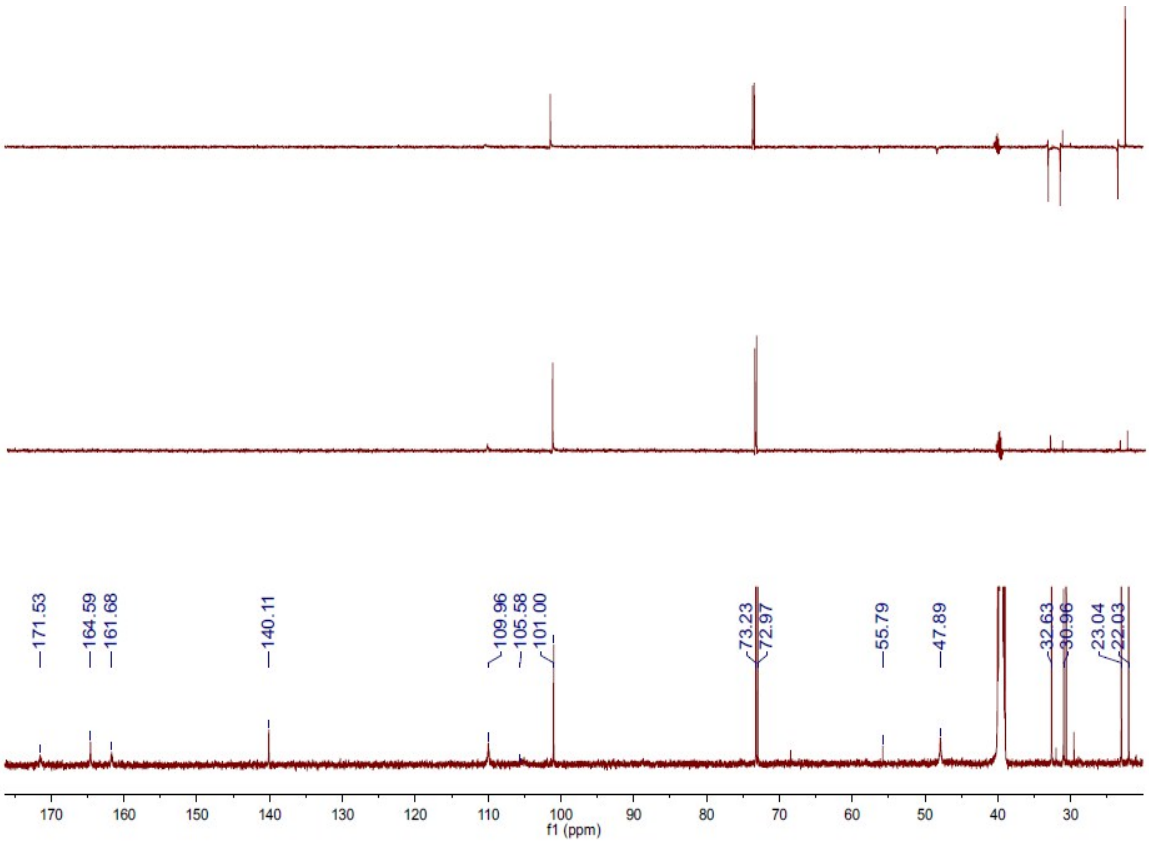

Figure S13. ^{1}H-^{1}H COSY spectrum of compound **5**.

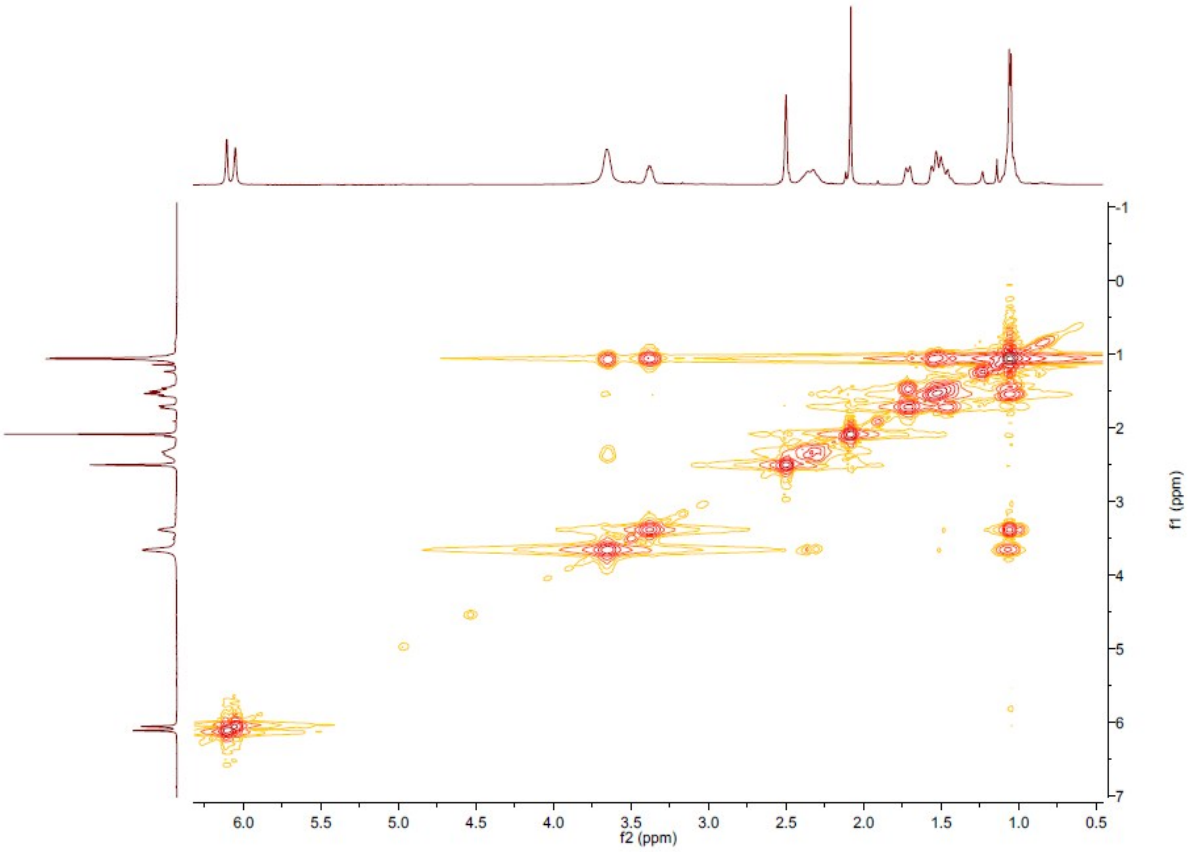

Figure S14. HSQC spectrum of compound **5**.

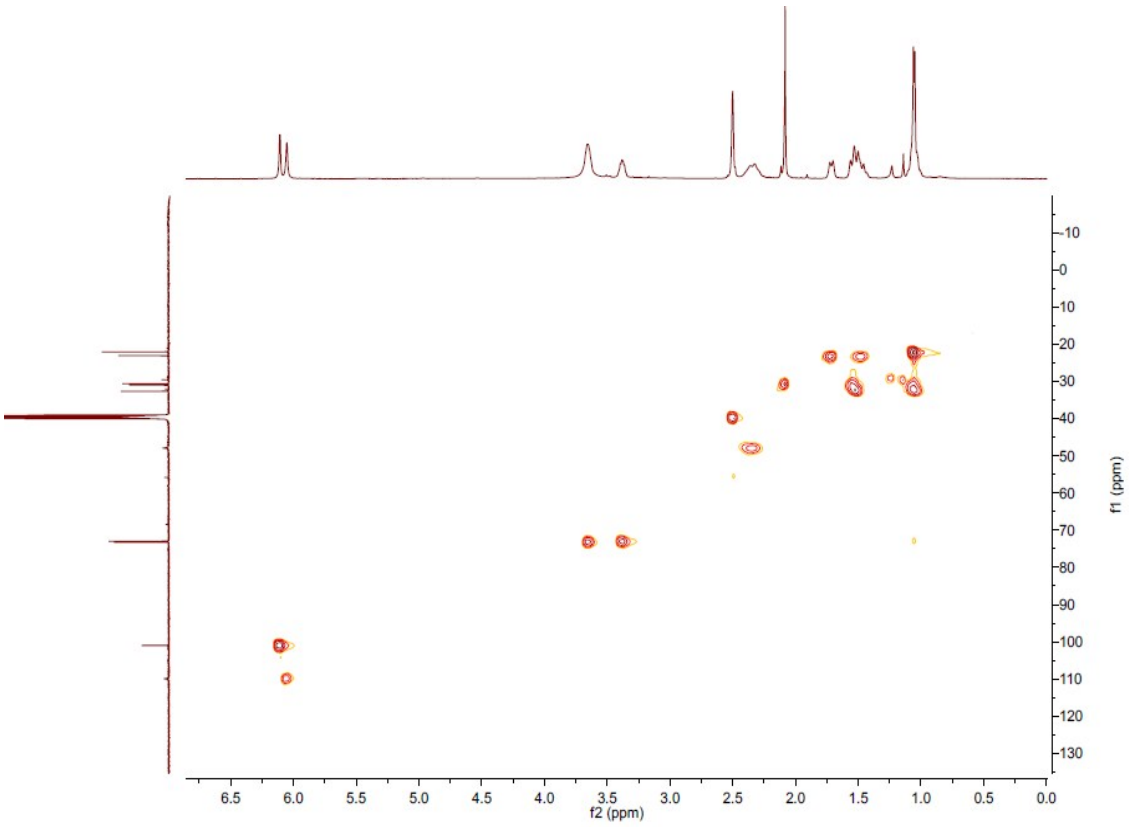

Figure S15. HMBC spectrum of compound **5**.

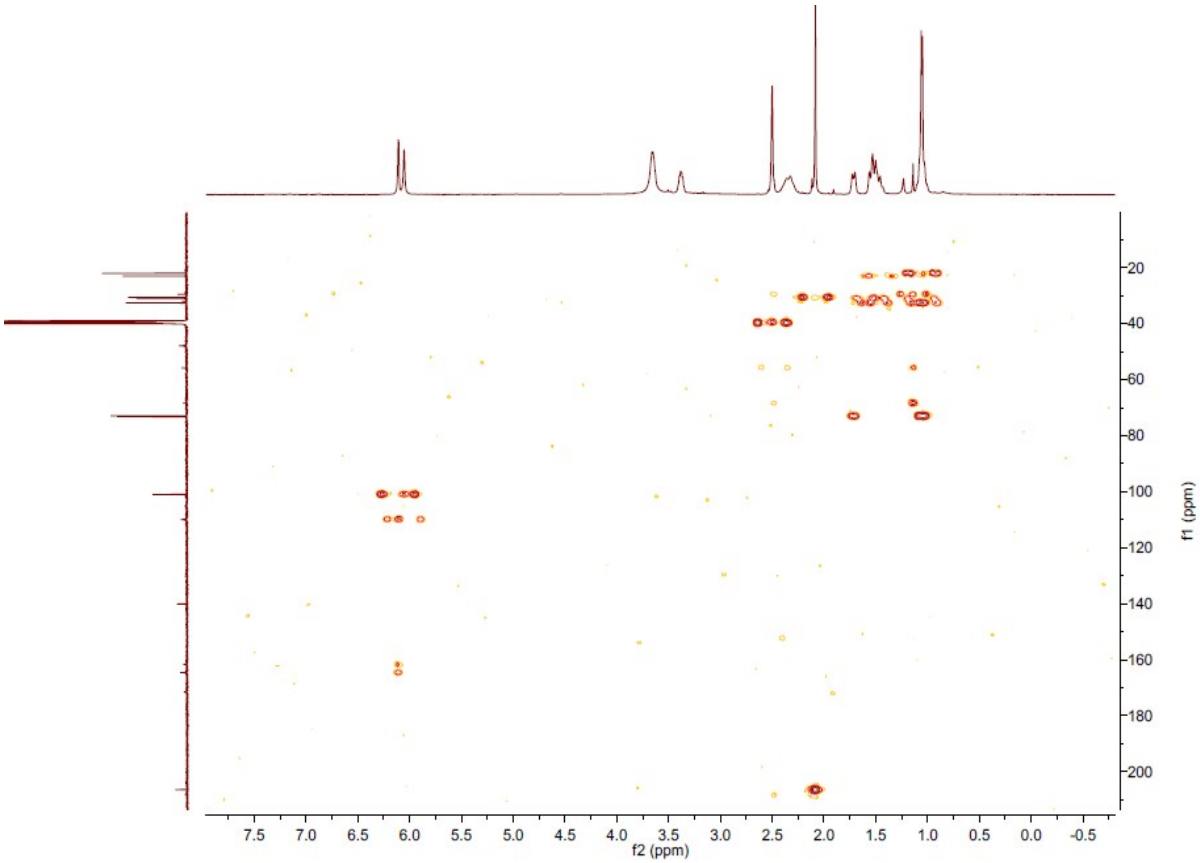

Figure S16. NOESY spectrum of compound **5**.

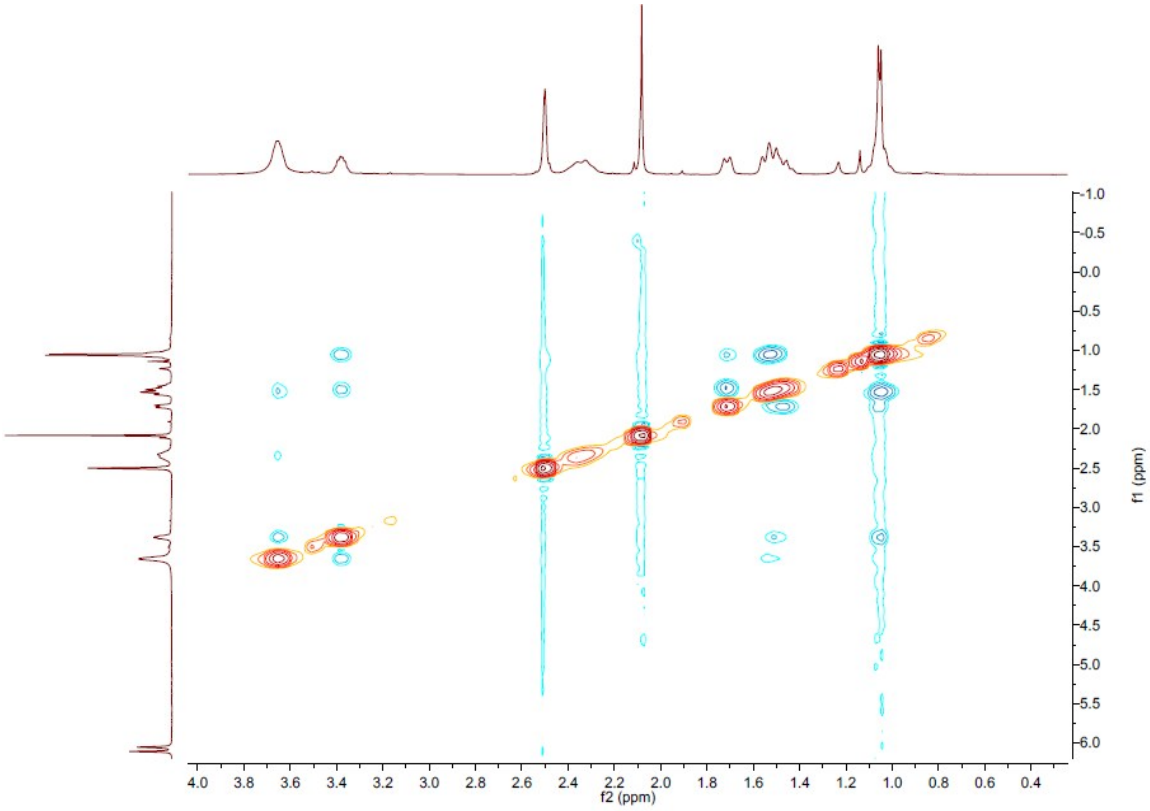

Figure S17. HR-ESI-MS spectrum of compound **6**.

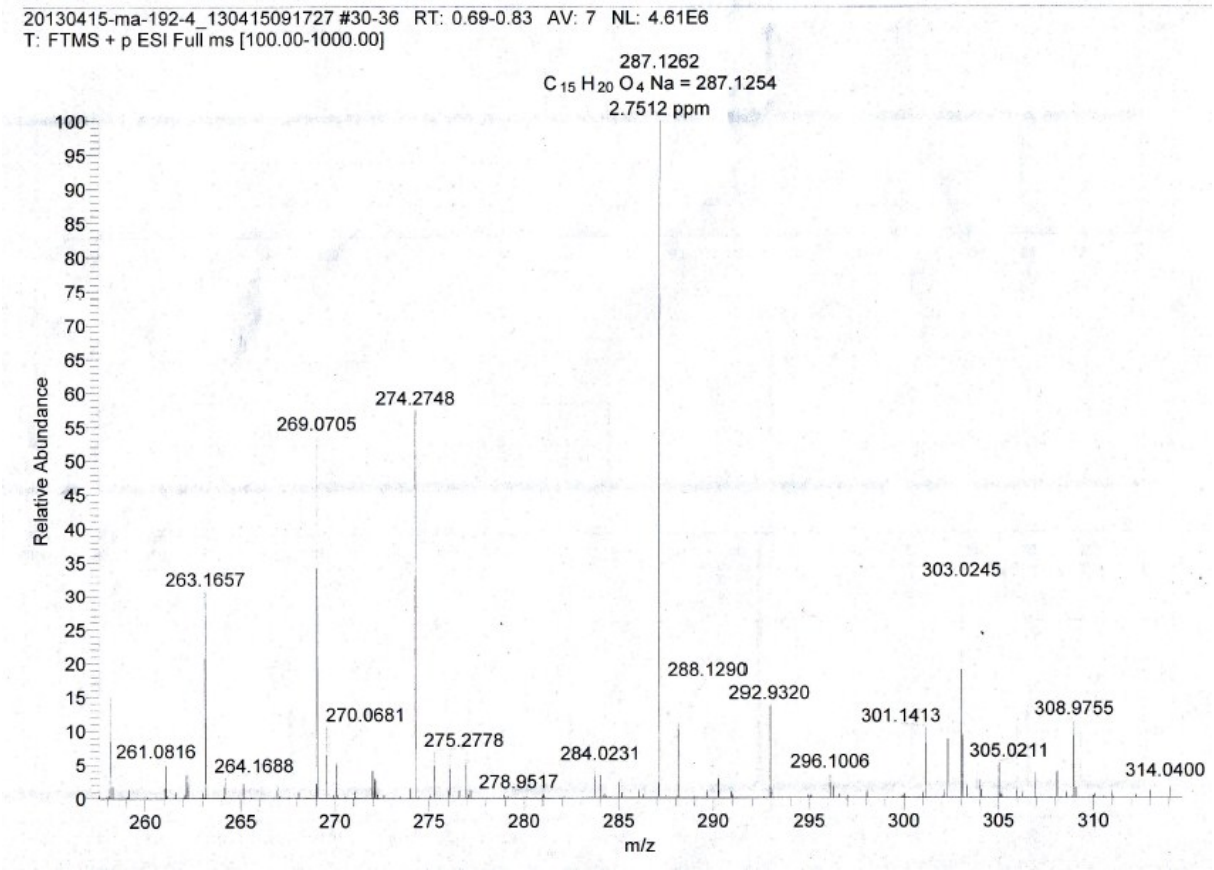

Figure S18. ^{1}H NMR (500M, $CDCl_3$) spectrum of compound **6**.

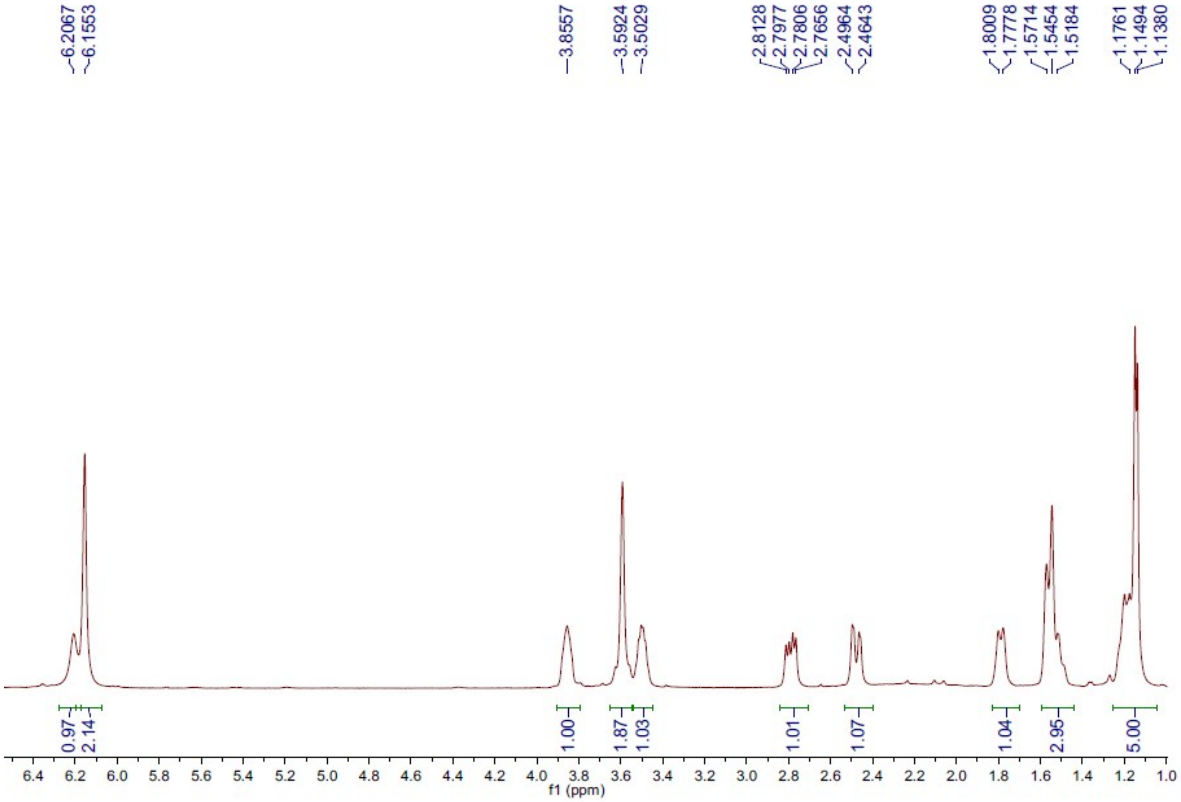

Figure S19. ^{13}C NMR (125M, $CDCl_3$) and DEPT spectra of compound **6**.

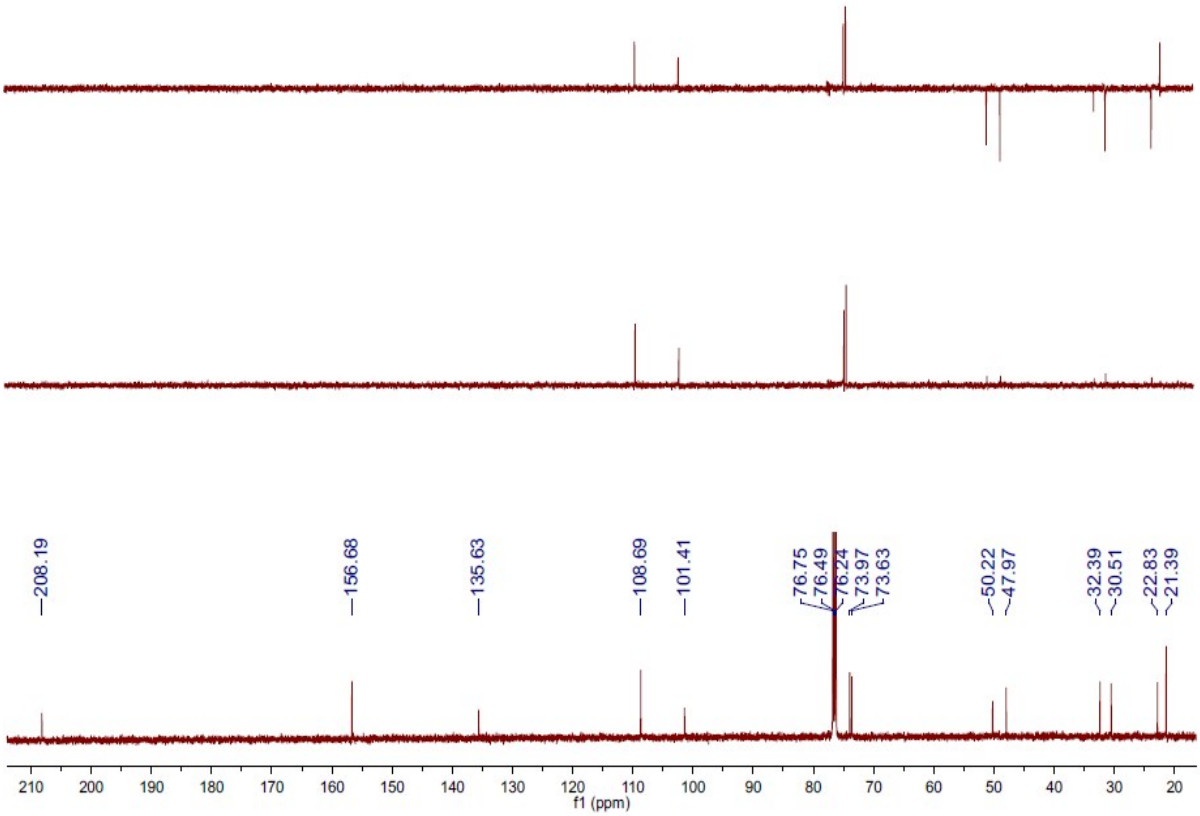

Figure S20. ^{1}H-^{1}H COSY spectrum of compound **6**.

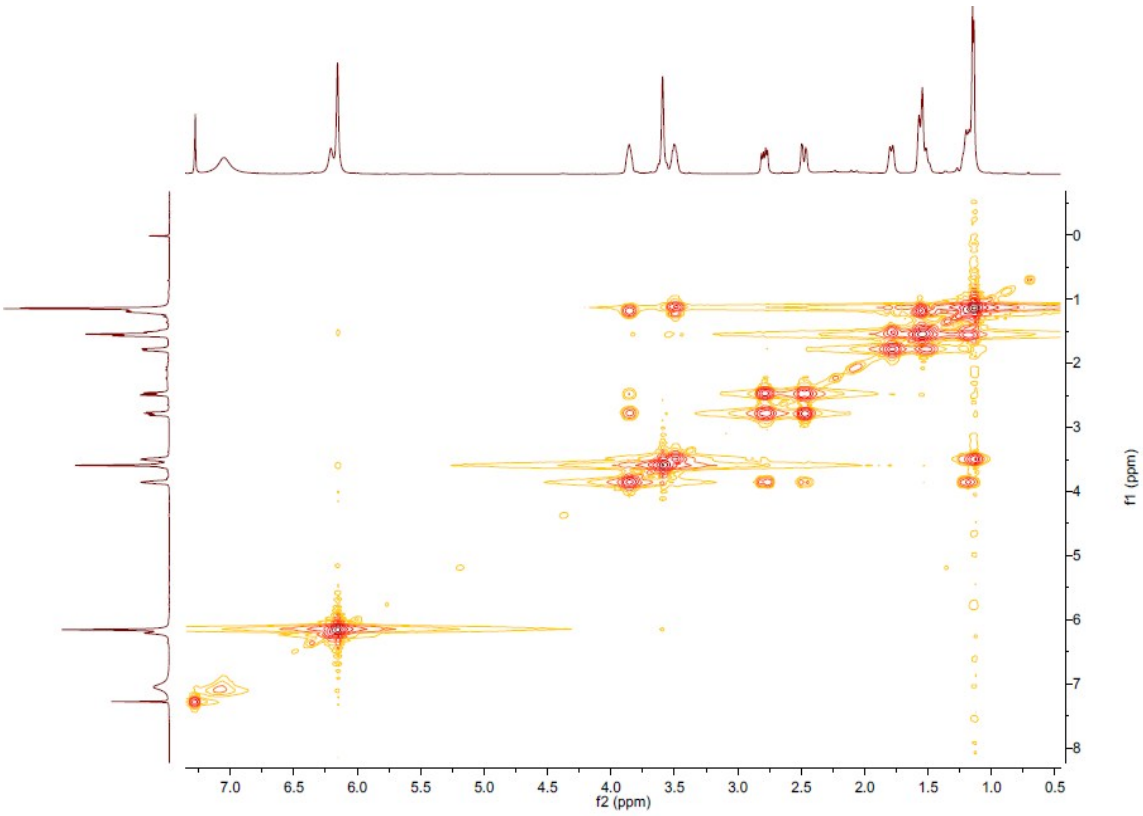

Figure S21. HSQC spectrum of compound **6**.

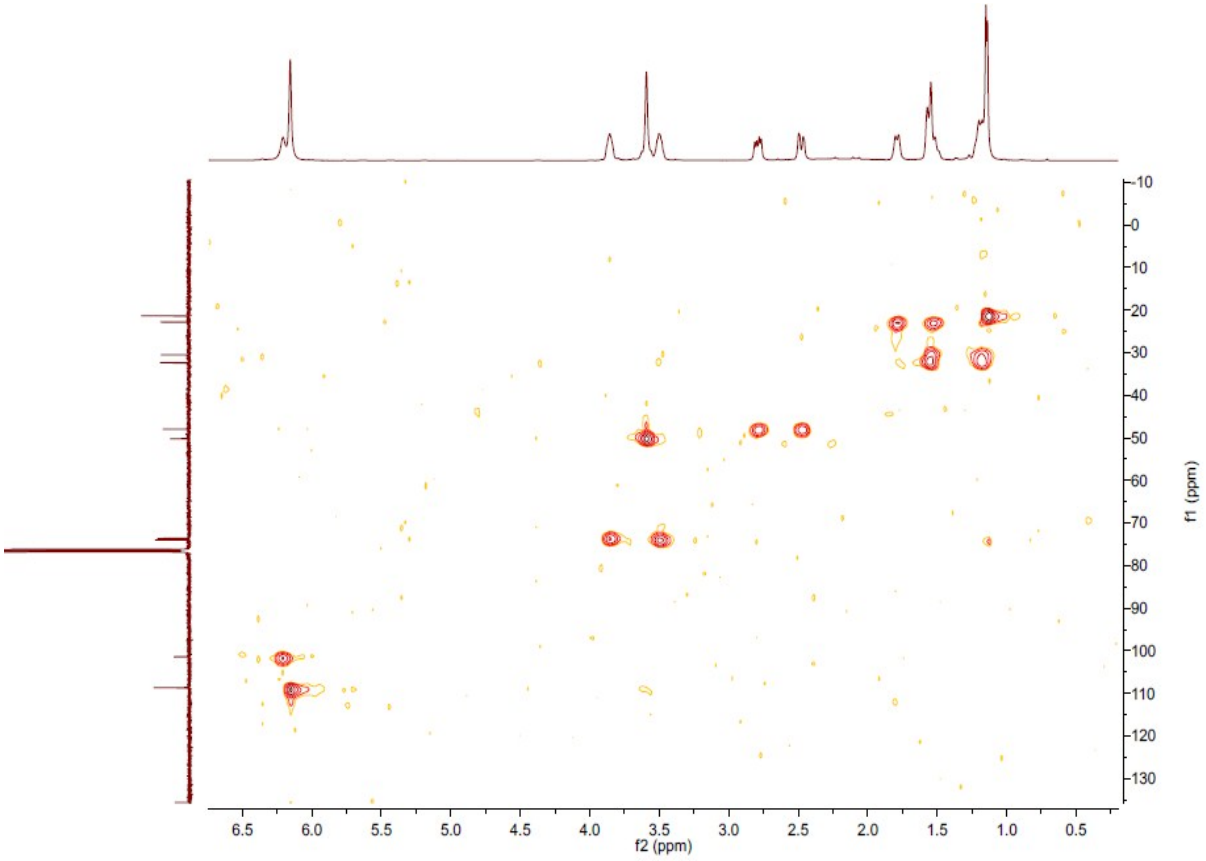

Figure S22. HMBC spectrum of compound **6**.

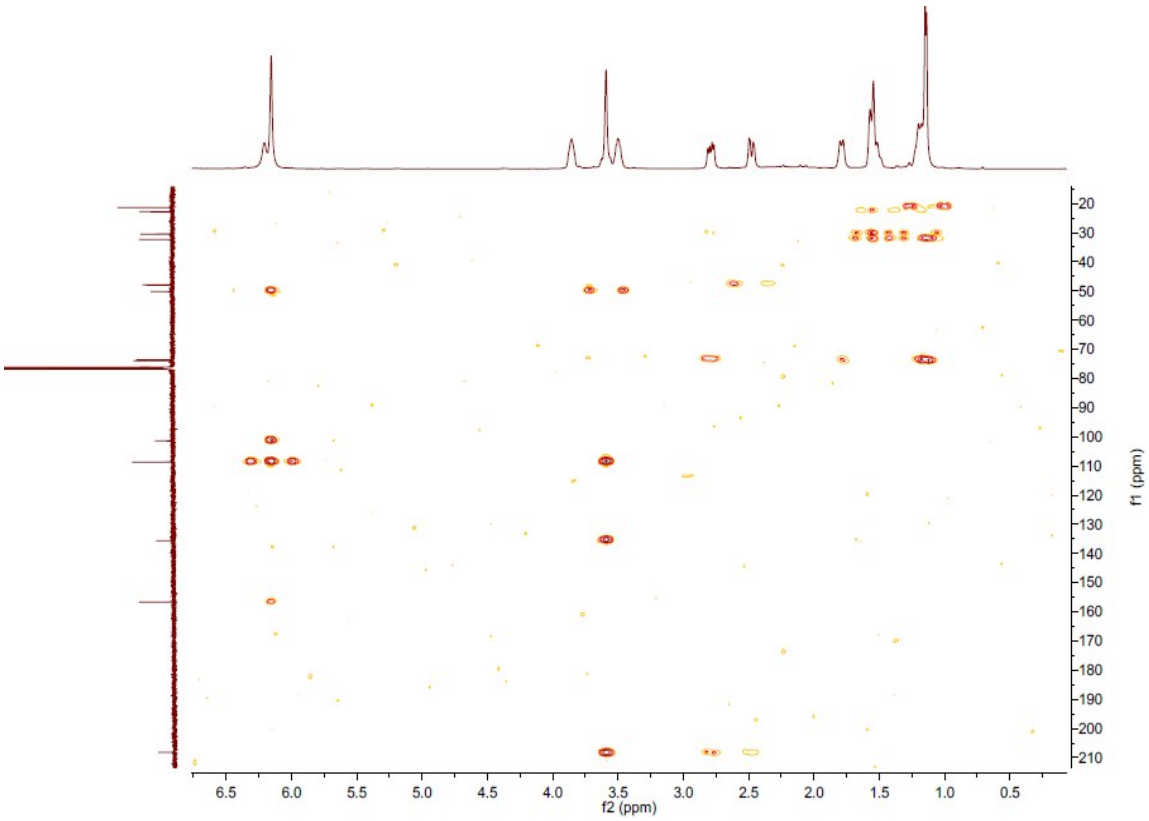

Figure S23. NOESY spectrum of compound **6**.

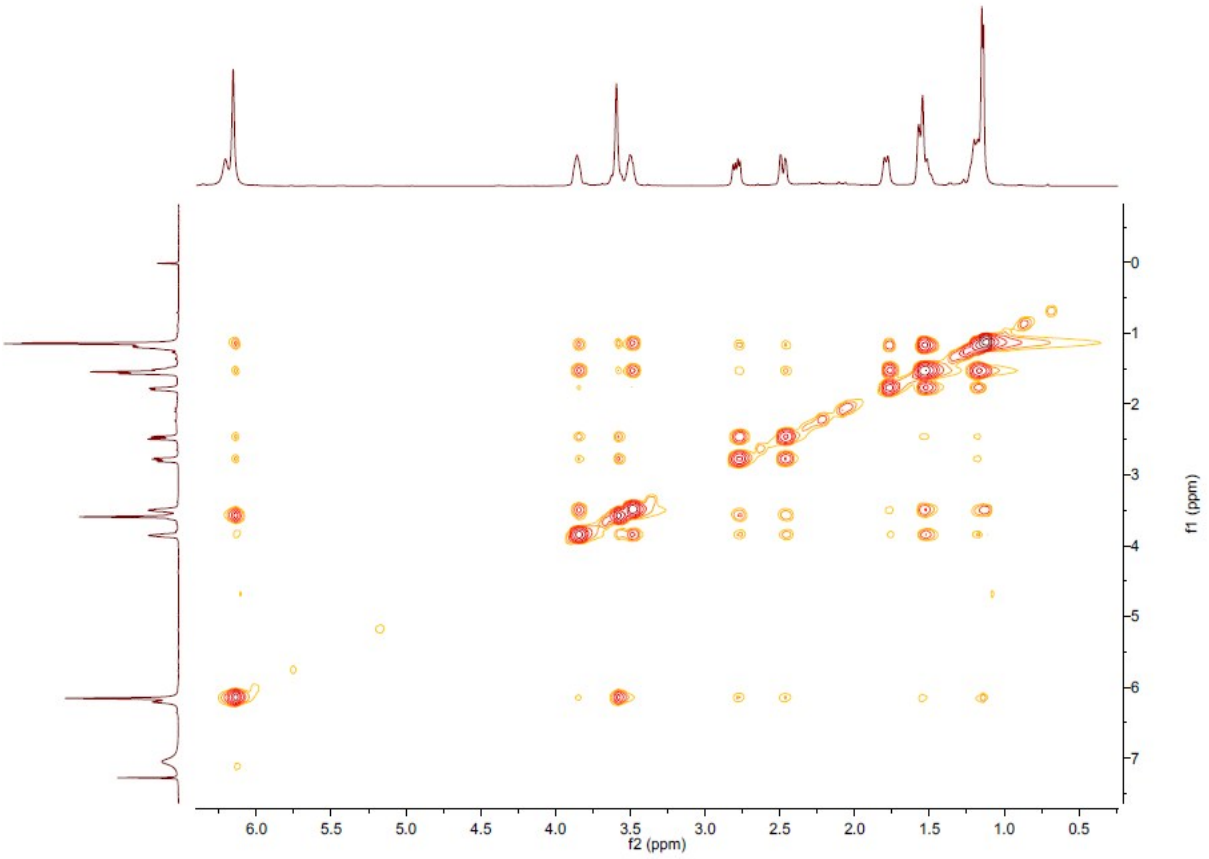

Figure S24. HR-ESI-MS spectrum of compound **7**.

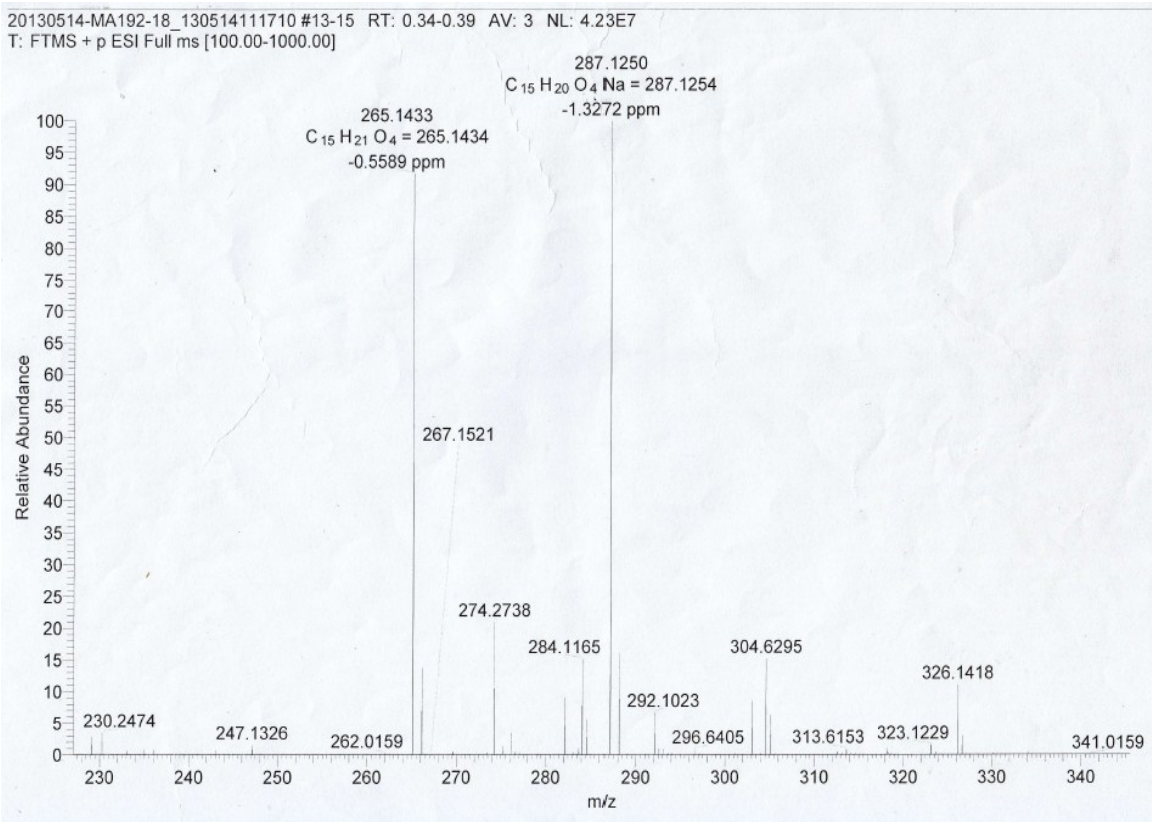

Figure S25. ^{1}H NMR (500M, acetone-d_6) spectrum of compound **7**.

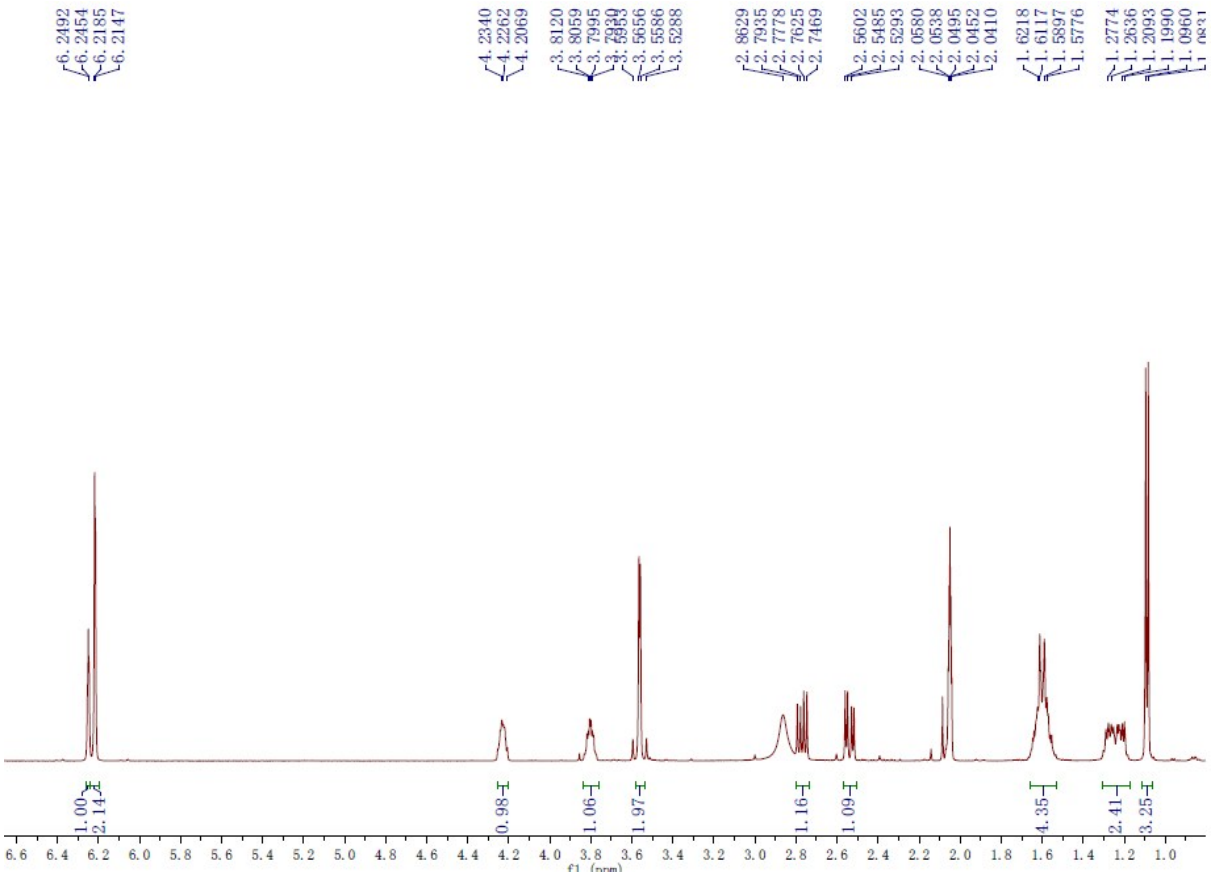

Figure S26. ^{13}C NMR (125M, acetone-d_6) and DEPT spectra of compound **7**.

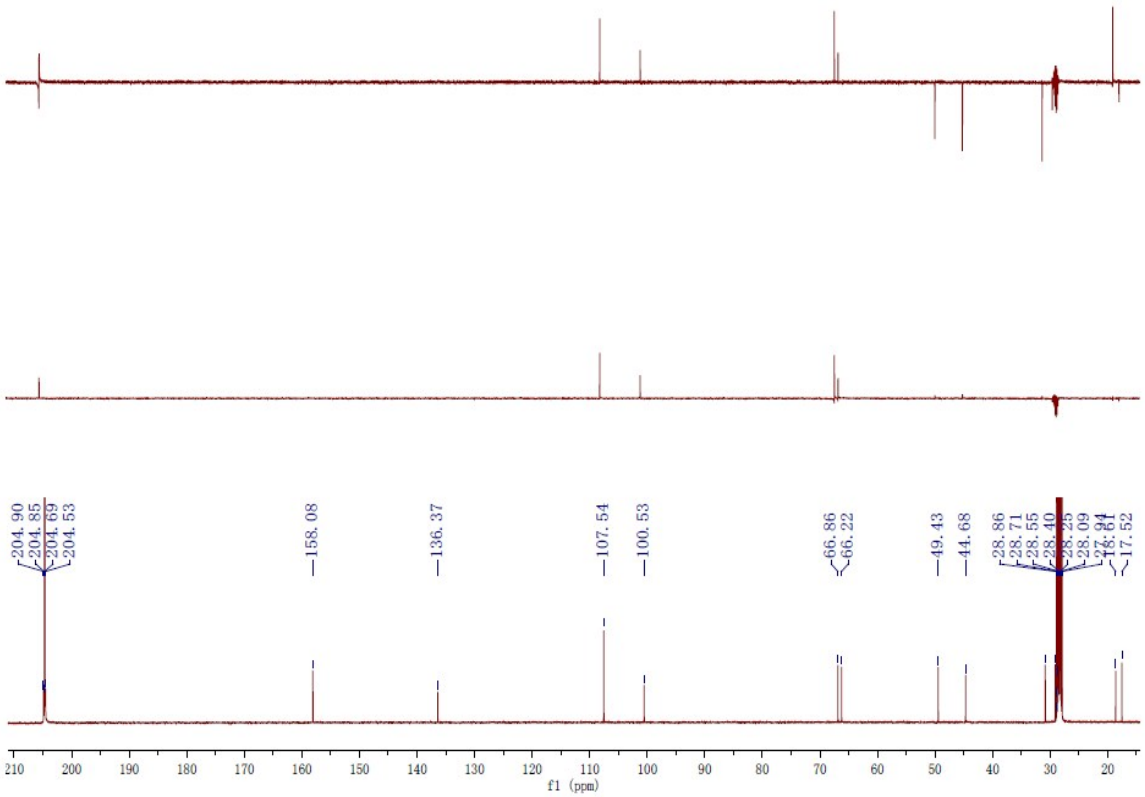

Figure S27. ^{1}H-^{1}H COSY spectrum of compound **7**.

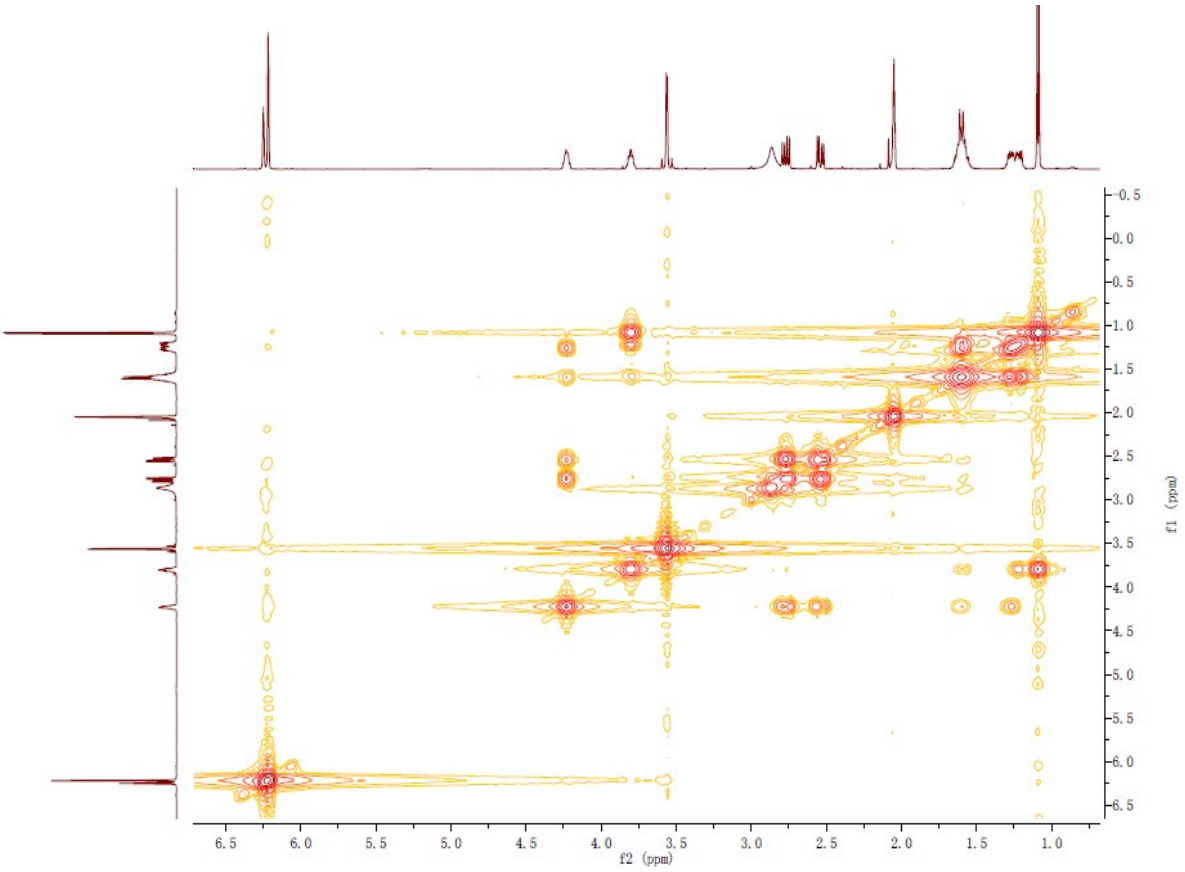

Figure S28. HSQC spectrum of compound **7**.

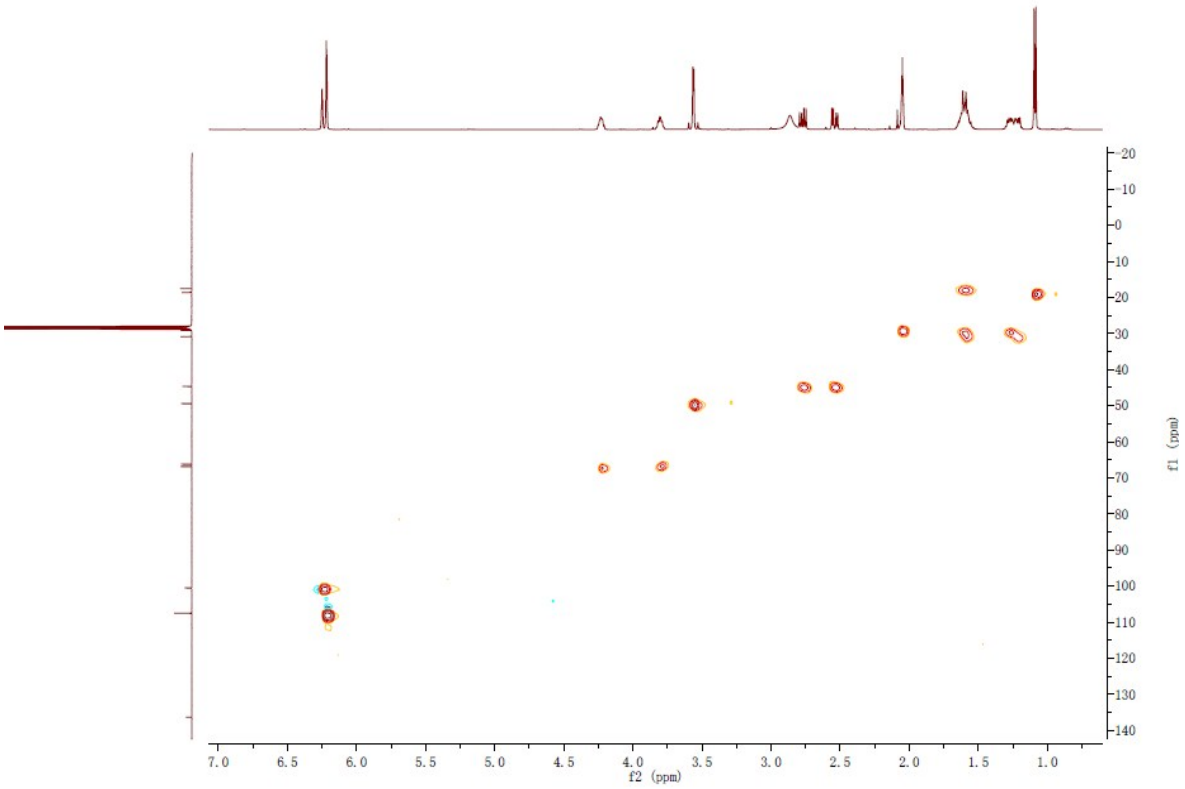

Figure S29. HMBC spectrum of compound **7**.

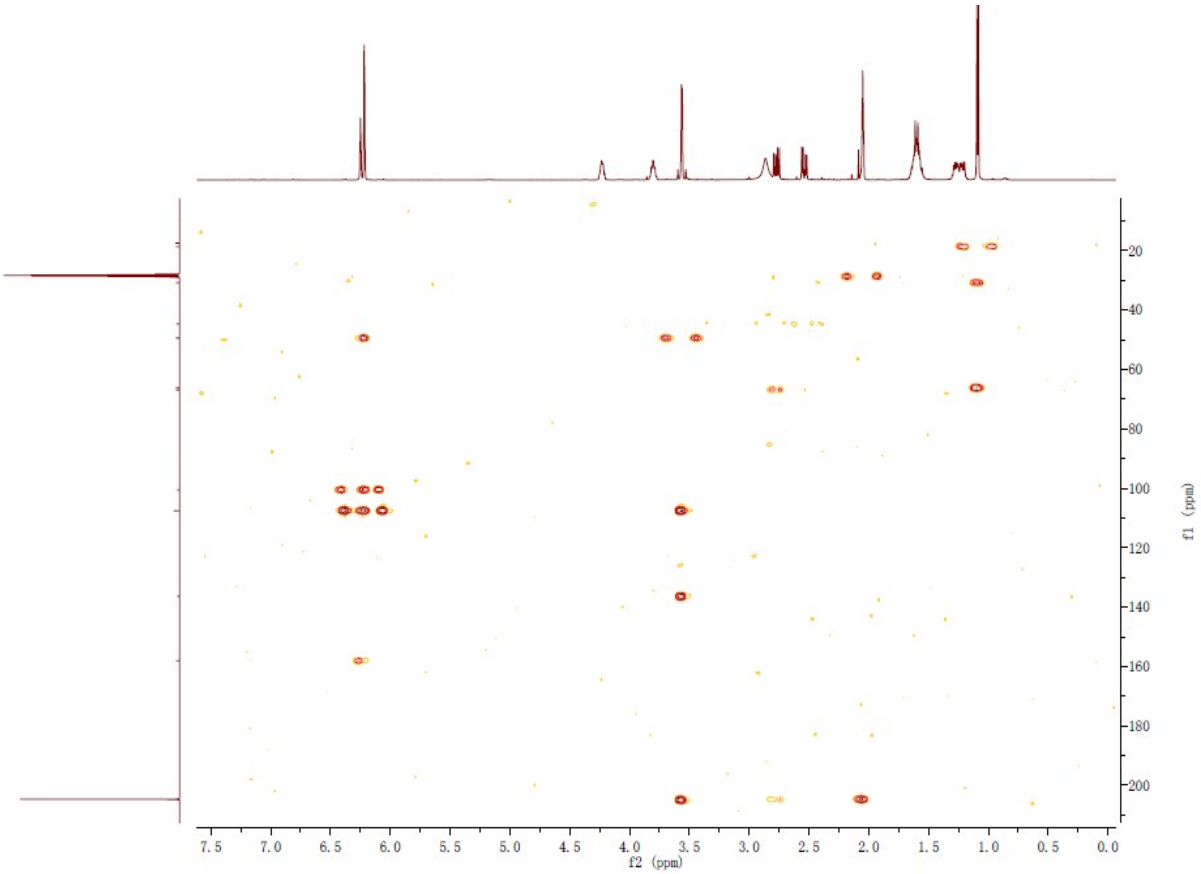

Figure S30. NOESY spectrum of compound **7**.

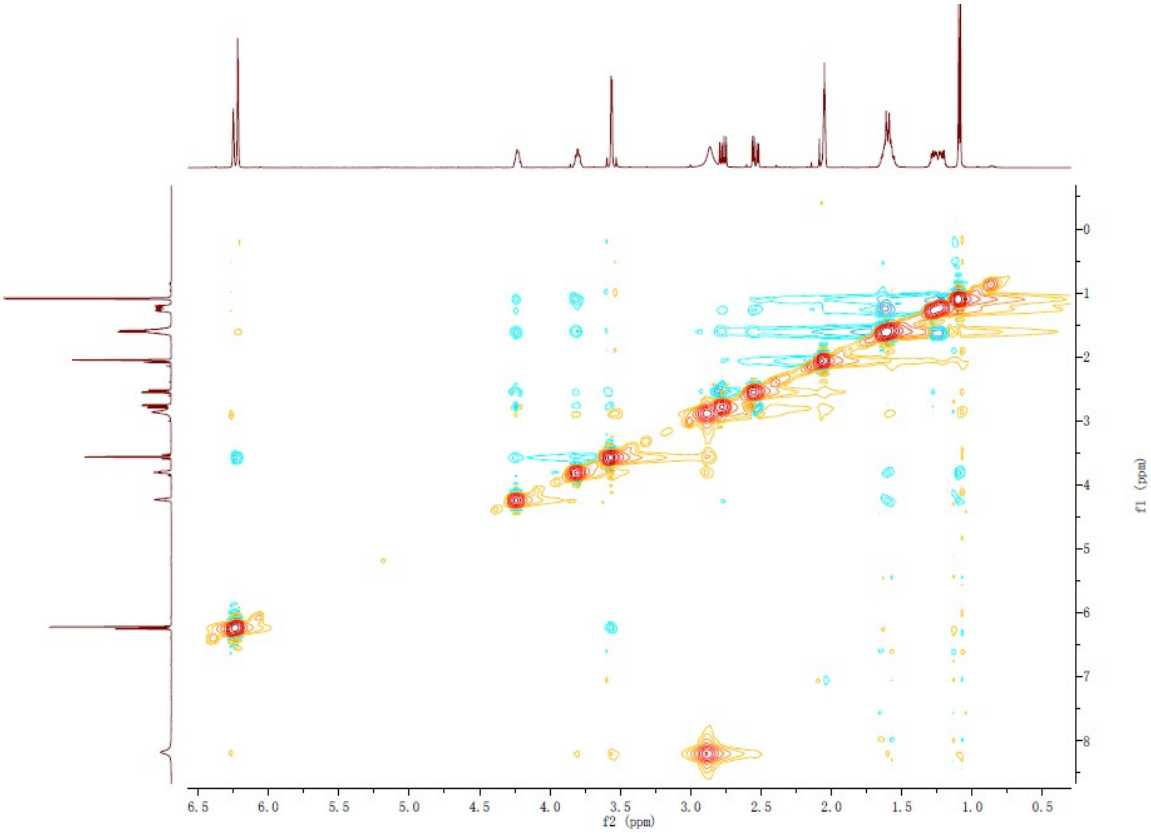

Figure S31. HR-ESI-MS spectrum of compound **8**.

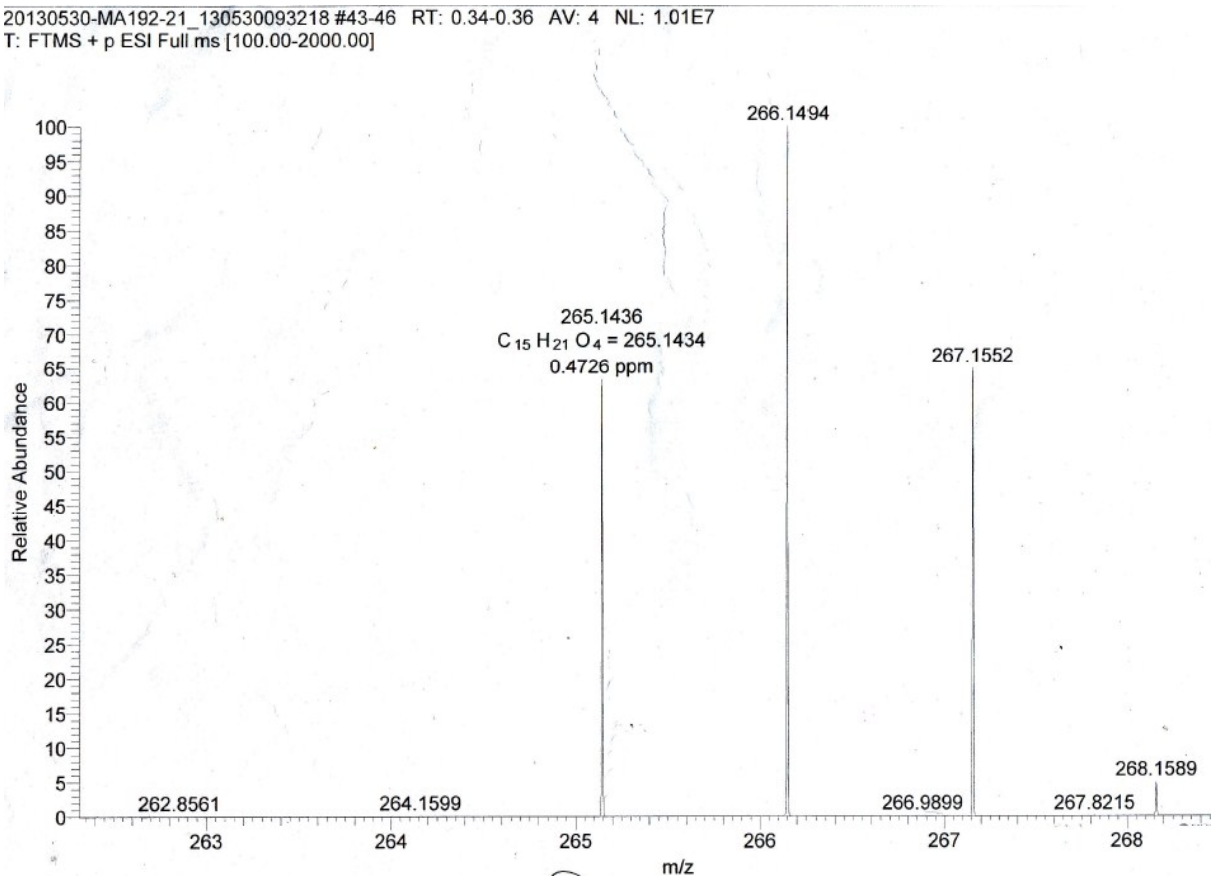

Figure S32. ^{1}H NMR (500M, $CDCl_3$) spectrum of compound **8**.

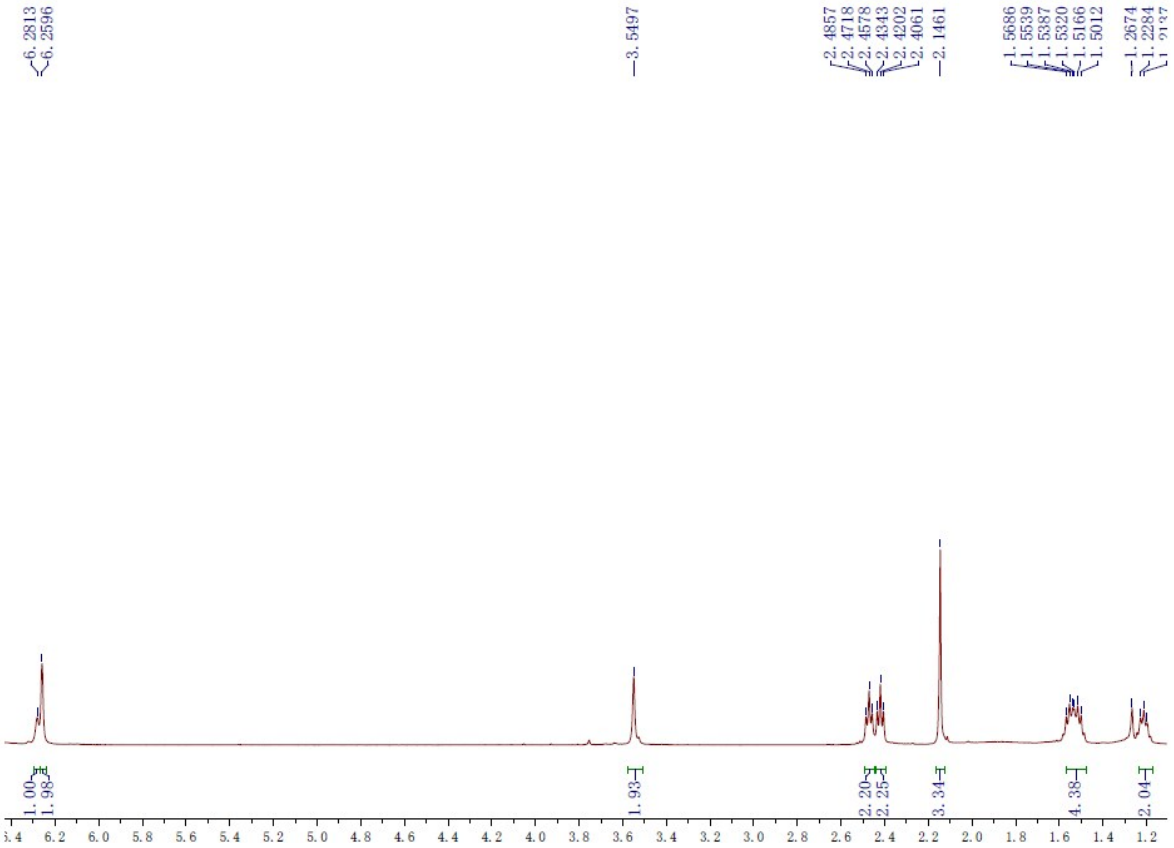

Figure S33. ^{13}C NMR (125M, $CDCl_3$) and DEPT spectra of compound **8**.

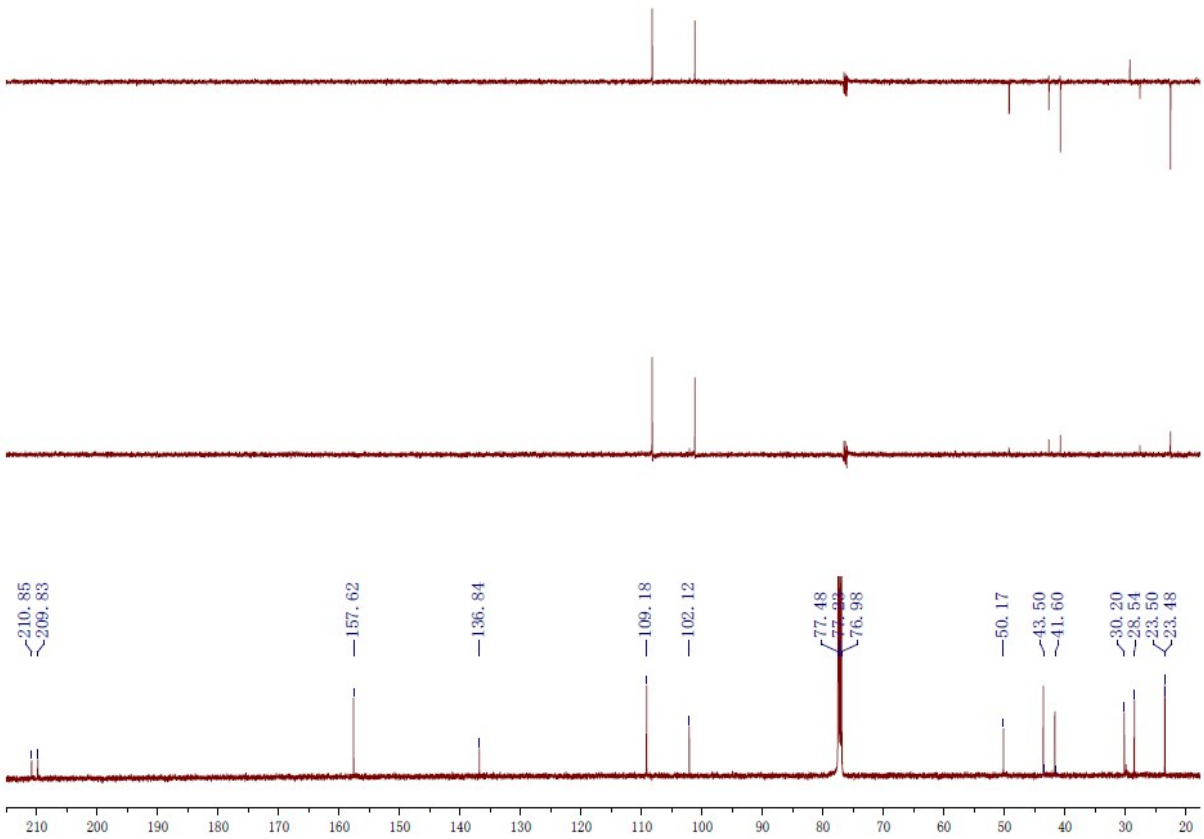

Figure S34. ^{1}H-^{1}H COSY spectrum of compound **8**.

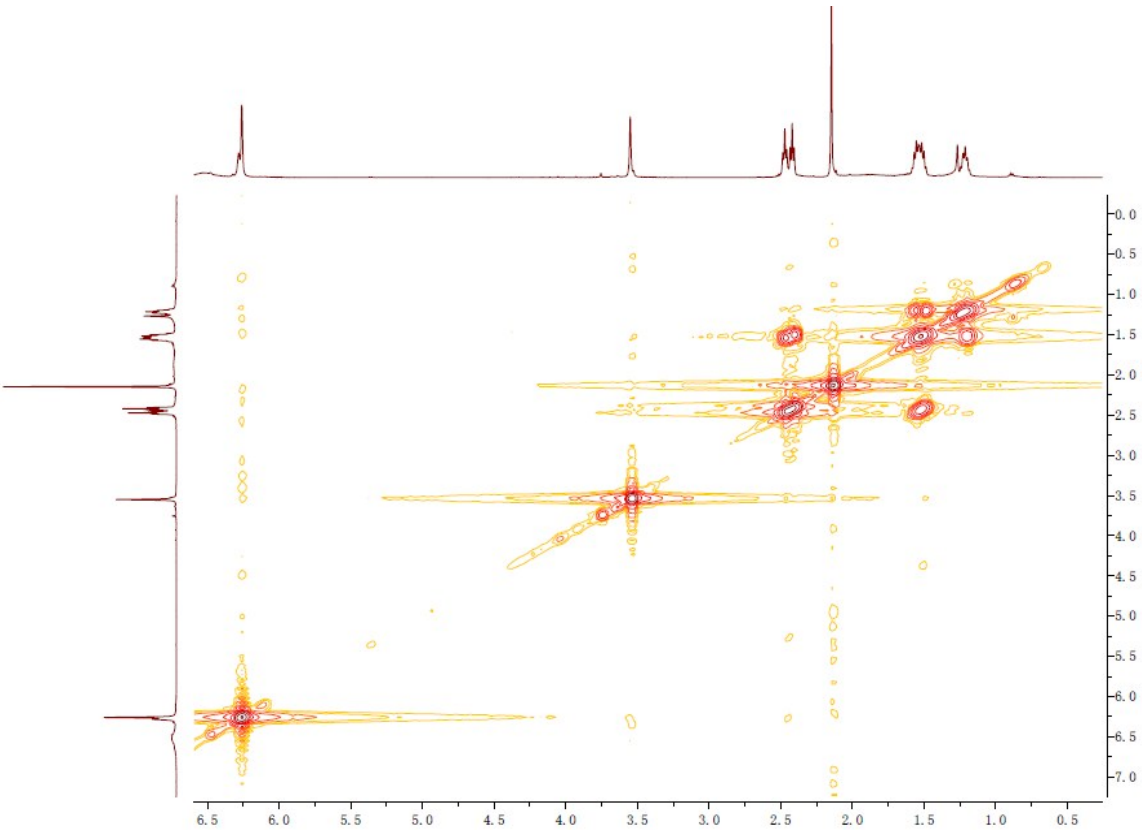

Figure S35. HSQC spectrum of compound **8**.

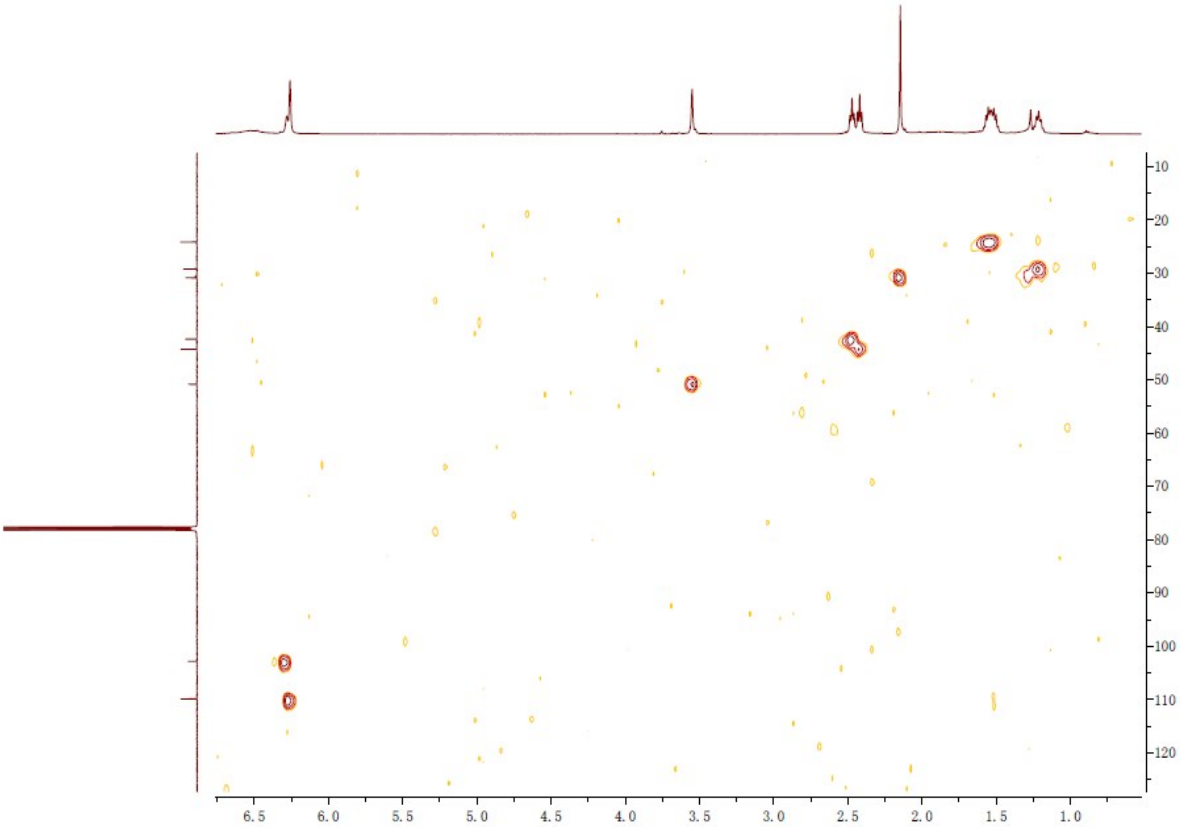

Figure S36. HMBC spectrum of compound **8**.

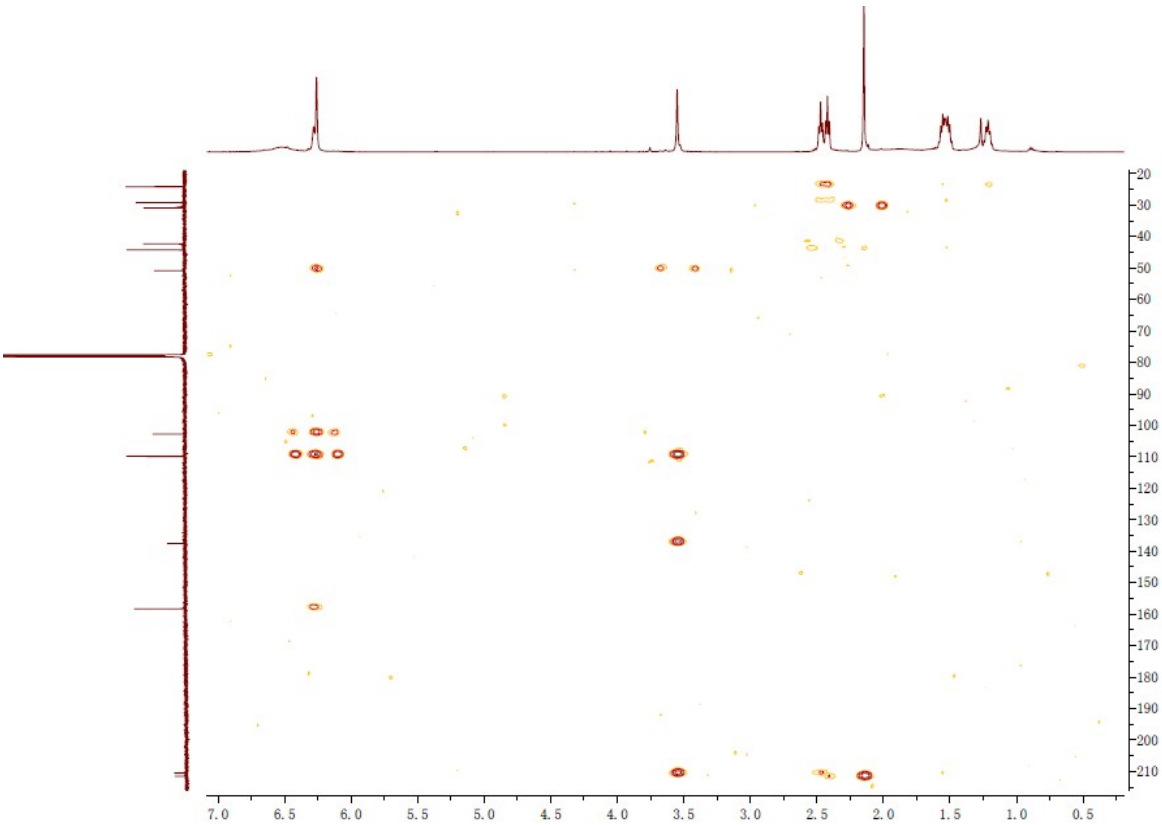

Figure S37. HR-ESI-MS spectrum of compound **9**.

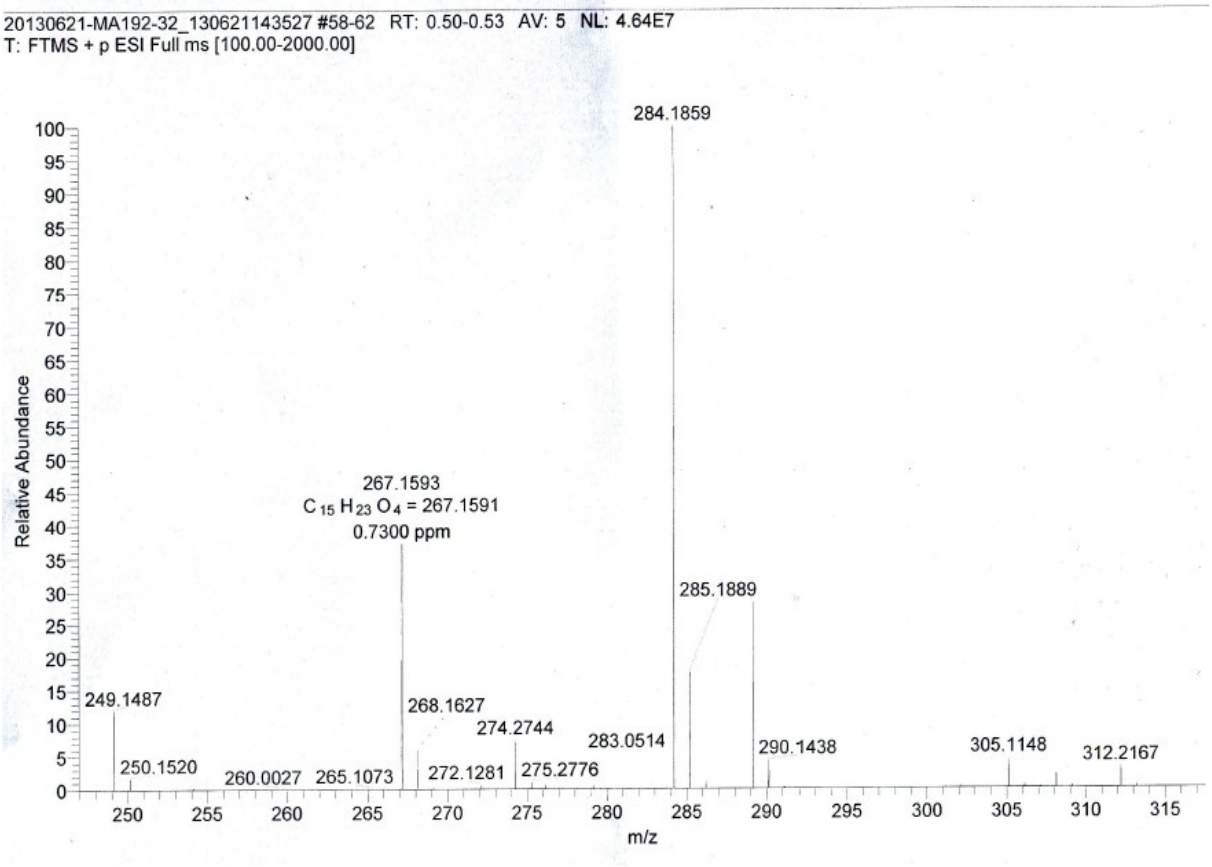

Figure S38. ^{1}H NMR (500M, DMSO-d_6) spectrum of compound **9**.

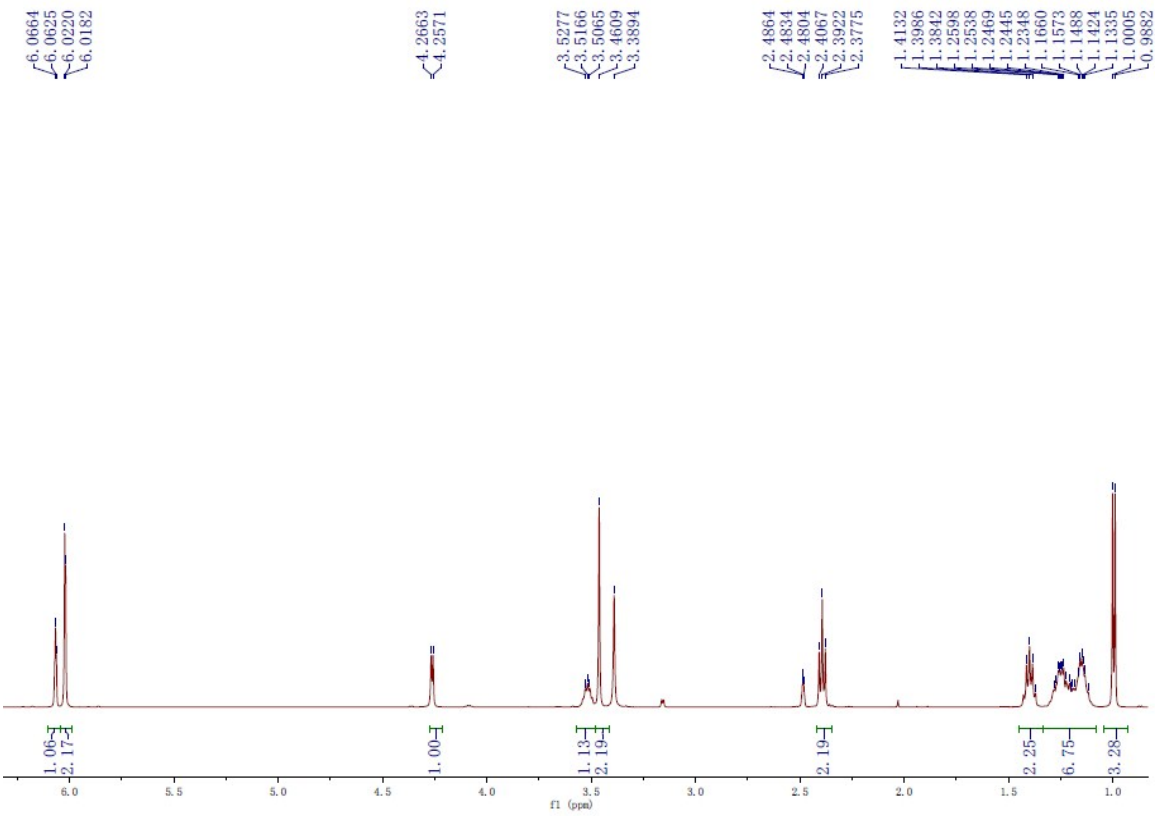

Figure S39. ^{13}C NMR (125M, DMSO-d_6) and DEPT spectra of compound **9**.

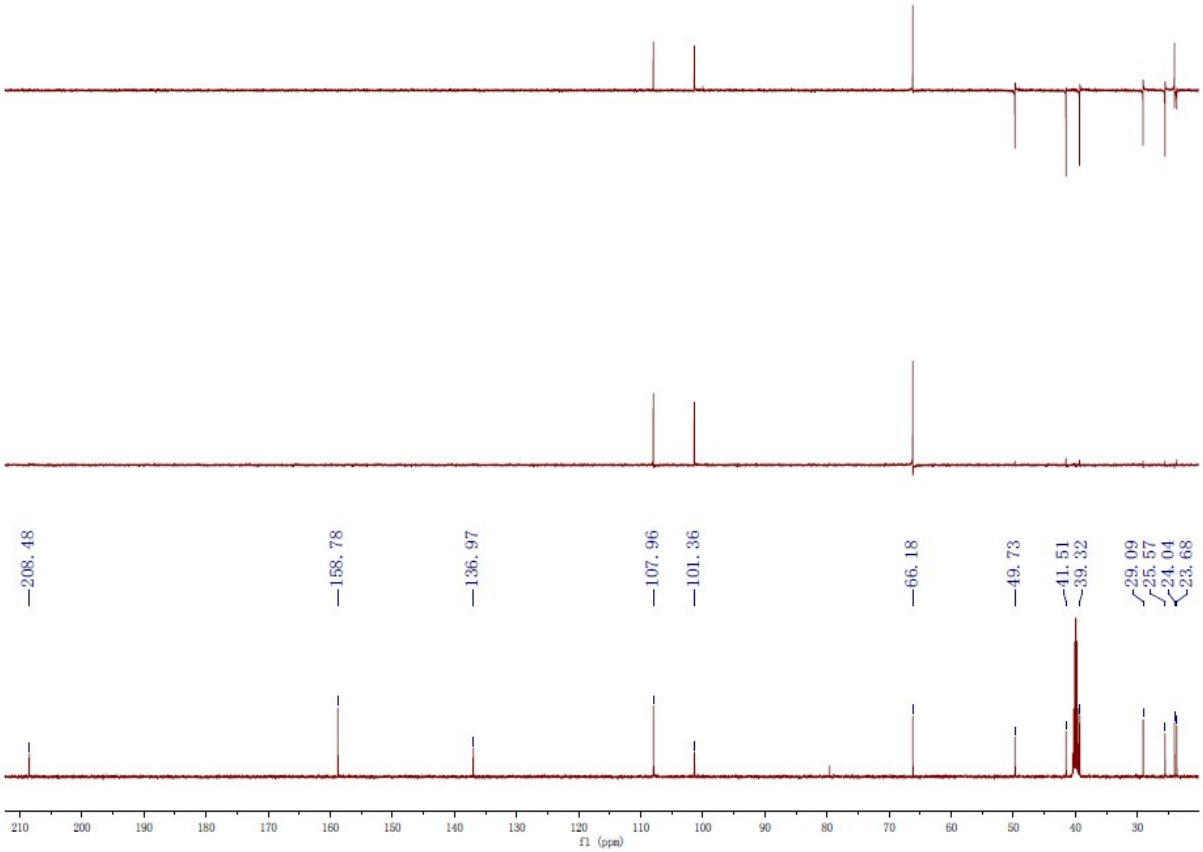

Figure S40. ^{1}H-^{1}H COSY spectrum of compound **9**.

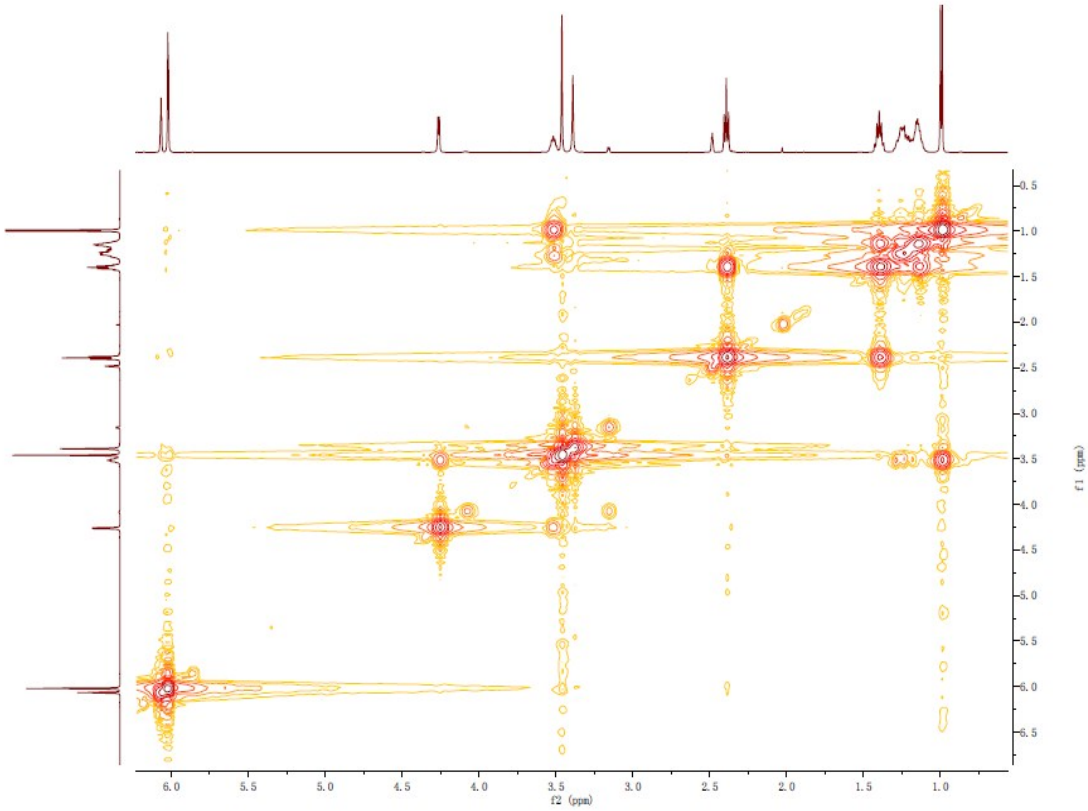

Figure S41. HSQC spectrum of compound **9**.

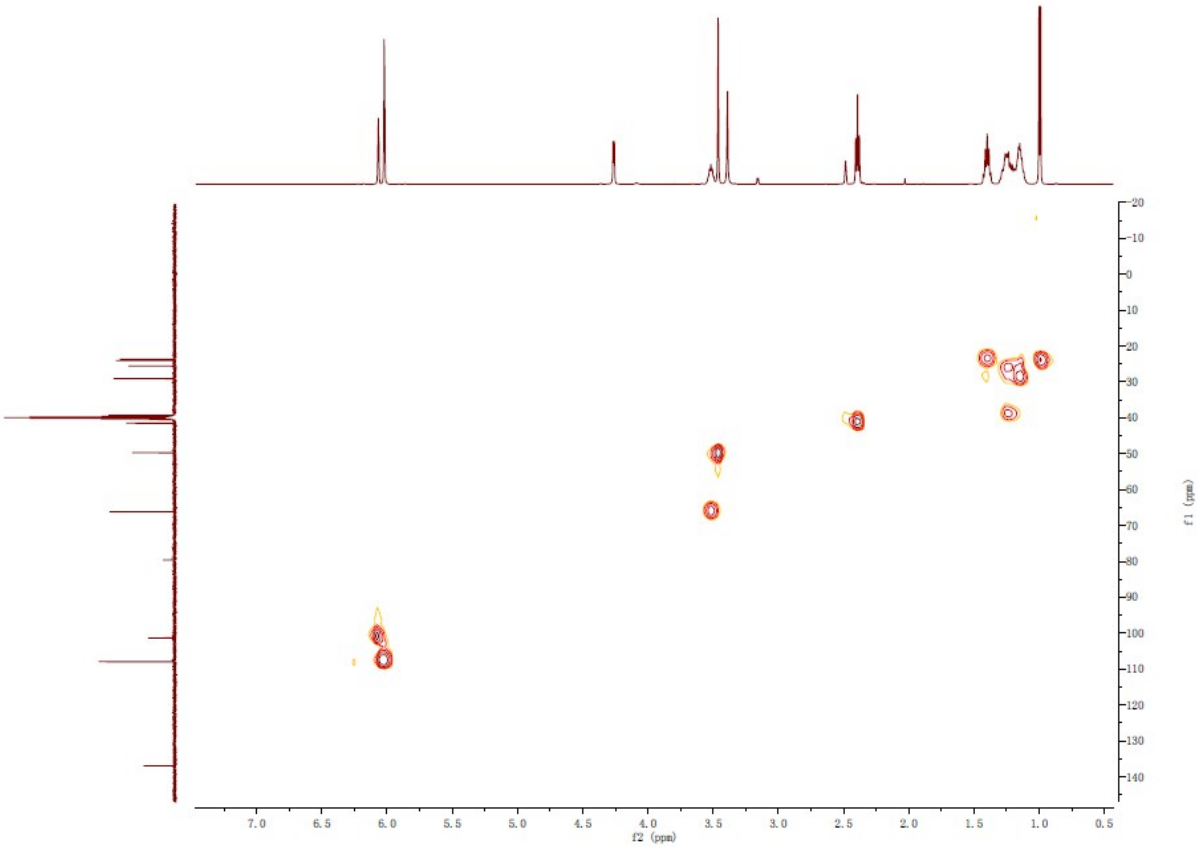

Figure S42. HMBC spectrum of compound **9**.

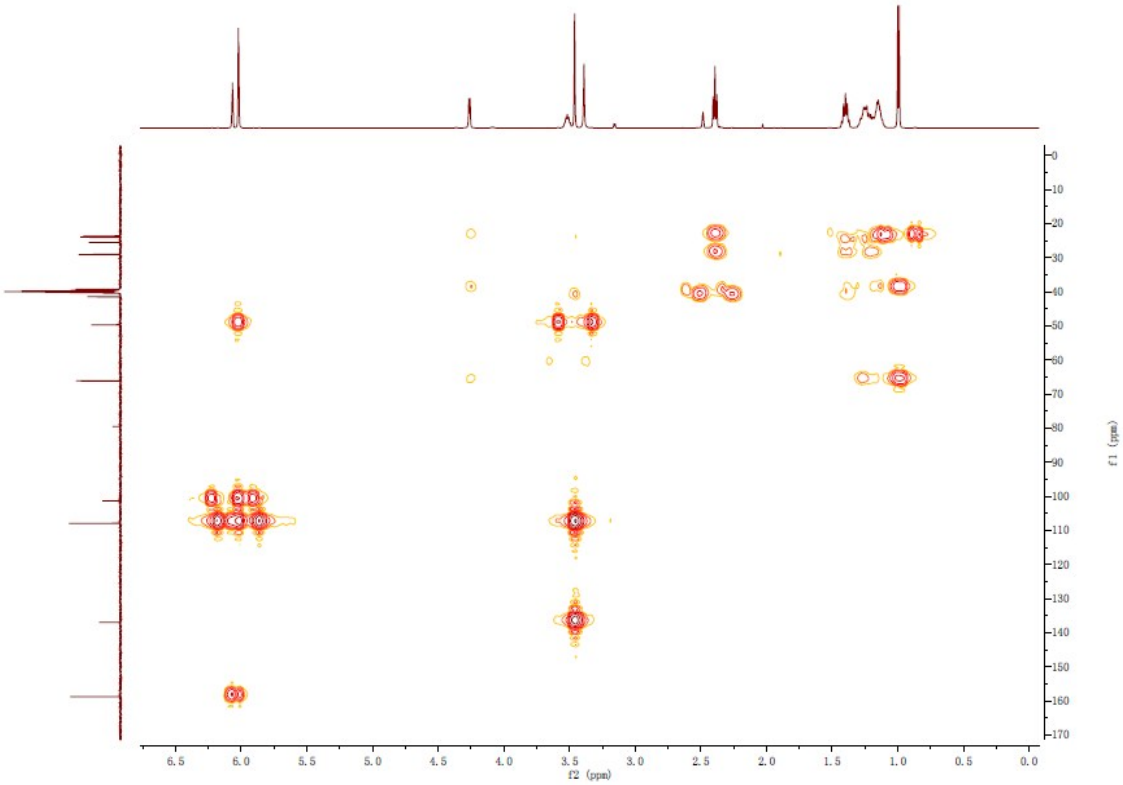

Figure S43: Decoupling spectrum of compound **4** (600M Hz, acetonitrile-d_3).